CHAPTER 4

RESULTS AND DISCUSSION

4.1 Preparation of FG

Results of the experiment were summarized in Table 4.1. Considering from the color of residue, working conditions and % recovery, it was found that the FG which was crushed to pass 200 mesh sieve, washed with distilled water and 3 M sulfuric acid (volume ratio of 3:1) gave the best results. Fig. 4.1 shows the illustration of the segregation sequence in the process of washing.

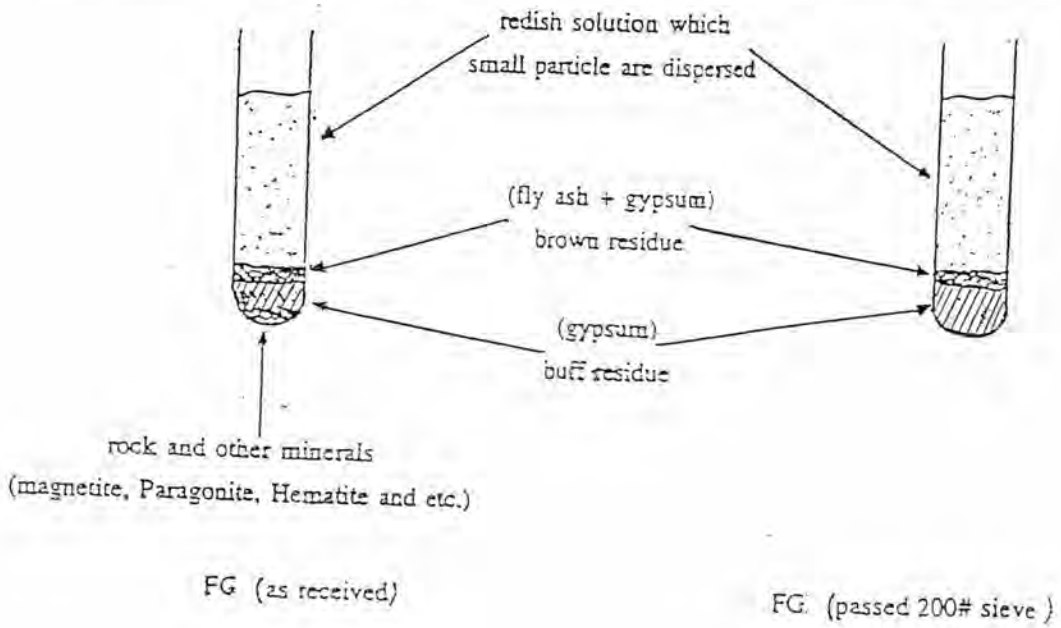

Fig. 4.1 Sequence of segregation.

Table 4.1 Washing conditions of FG.

Suspension (5 ml.)	Conditions			Residue	
	H_2SO_4 3 M (ml)		H_2O_2 20% (ml)	Color	Recovery (wt%)
	T_{room} (27°C)	100°C	T_{room} (27°C)		
FG (as received)	0.00	-	-	brown	95.0
	0.25	-	-	brown	83.0
	0.50	-	-	brown	58.0
	1.00	-	-	light brown	62.0
	-	0.00	-	brown	94.0
	-	0.25	-	brown	68.0
	-	0.50	-	brown	71.0
	-	1.00	-	light brown	69.0
	-	-	0.25	brown	86.0
	-	-	0.50	brown	86.0
	-	-	1.00	brown	87.0
FG (-200 mesh)	0.25	-	-	light brown	87.0
	0.50	-	-	light brown	86.0
	1.00	-	-	buff	76.0
	-	0.25	-	brown	78.0
	-	0.50	-	light brown	82.0
	-	1.00	-	light brown	57.0
FG (-325 mesh)	0.25	-	-	light brown	65.0
	0.50	-	-	buff	73.0
	1.00	-	-	buff	58.0
	-	0.25	-	brown	65.0
	-	0.50	-	light brown	61.0
	-	1.00	-	buff	63.0

4.1.1 Characteristic of FG

a.) Phase present in FG powder

From the results of XRD and EDS investigations shown in Fig. 4.2 and 4.3, only gypsum was observed and no second phase present but the result from phase calculation (Appendix : Table 1, page 150) indicated that, there was small amount of other phases (4.45%) consisting in the FG.

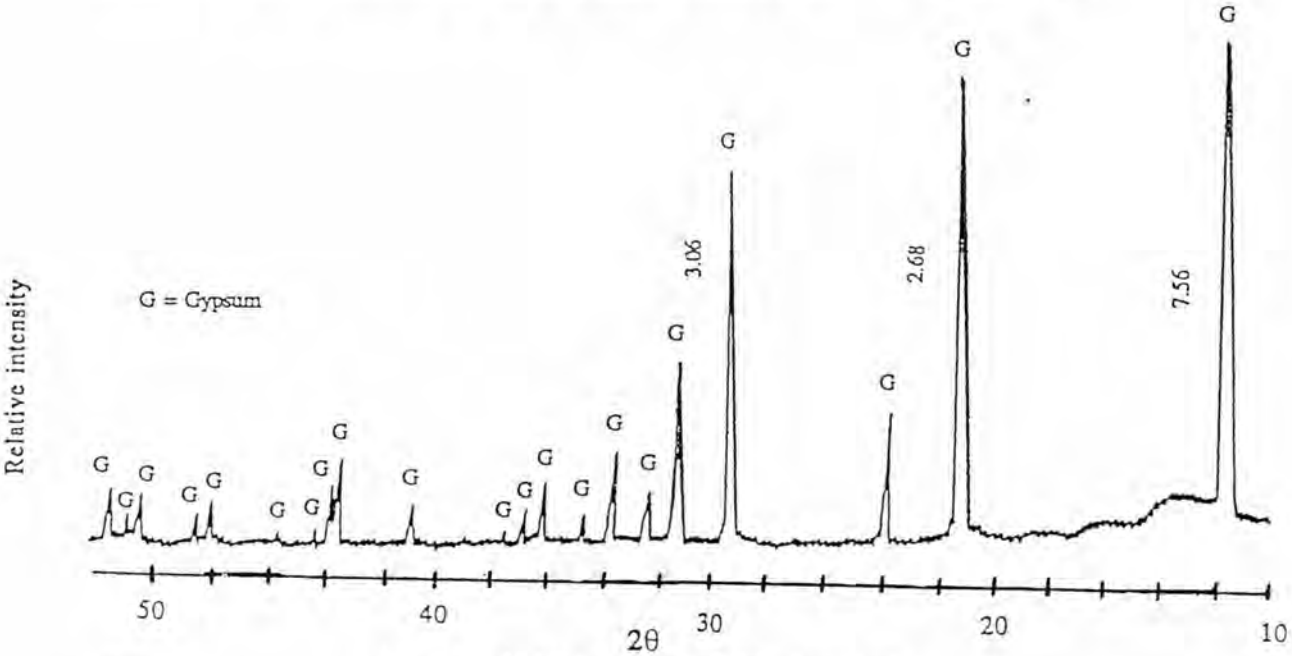

Fig. 4.2 XRD pattern of FG (washed).

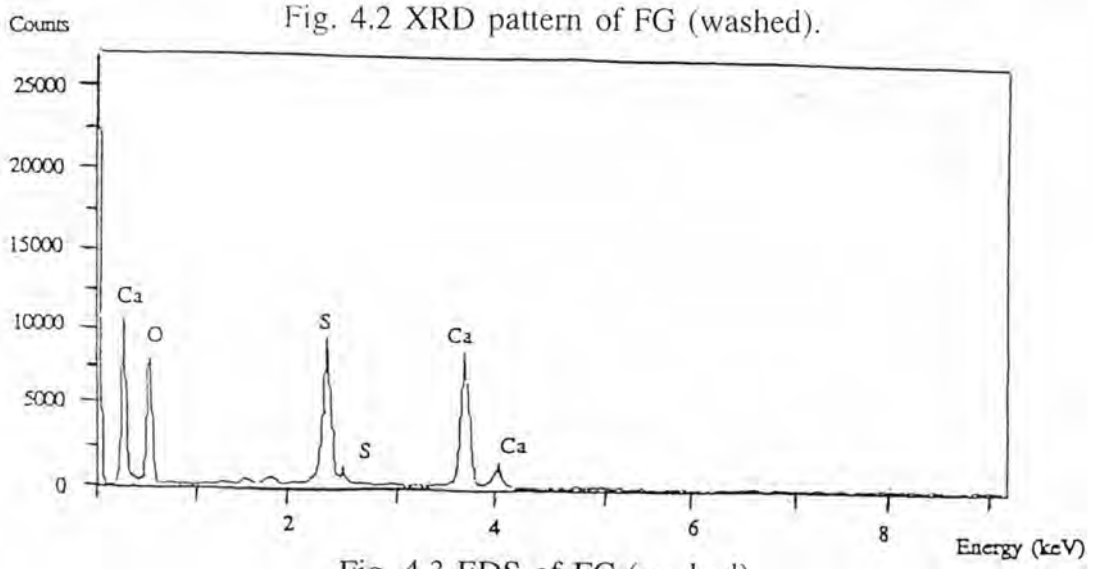

Fig. 4.3 EDS of FG (washed).

b.) Particle size distribution

Results from the paticle size analyzer were illustrated in Fig. 4.4.

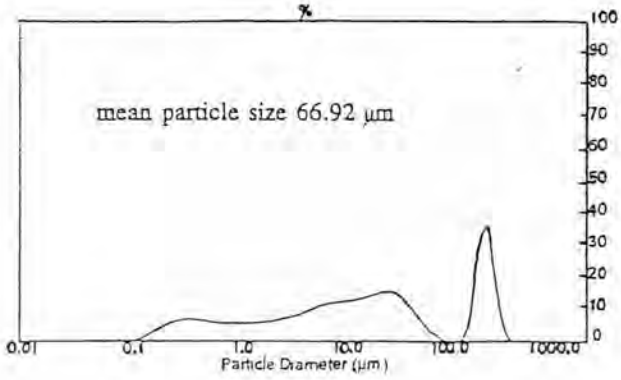

(a.)

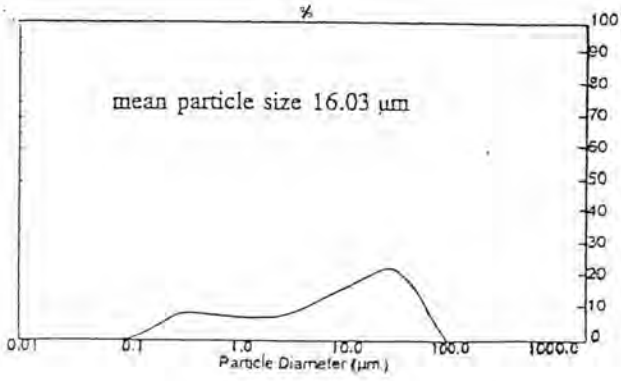

(b.)

Fig. 4.4 Particle size distribution curves of a.) FG (as received) and b.) FG (washed).

The particle size distribution curve of FG (as received) showed the discontinuity which was due to the difference in morphology of the two ranges of particles. It was obvious from the SEM micrographs Fig. 4.5 (a.) that the as received FG was original rod shaped crystal, over 100 µm in size and was later broken down into smaller and more rounded particles as shown in Fig. 4.5 (b.) in which the as received FG was crushed to pass 200 mesh sieve prior to washing.

c.) Particle morphology

SEM micrographs of FG powders were shown in Fig. 4.5. Both FG powder were originally rod shaped particles and become more rounded after breaking down. The SEM results confirmed that the particle size distribution range of the as received FG was very large compared to that of the washed FG.

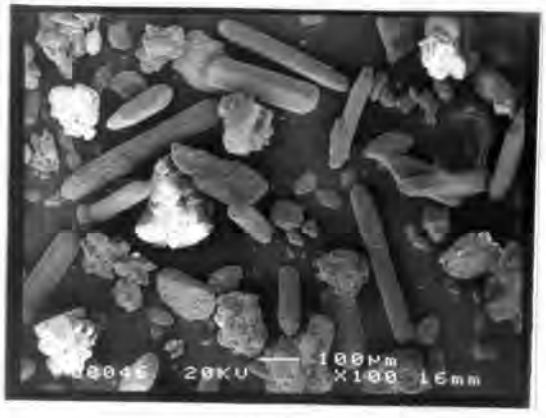

(a.)

(b.)

Fig. 4.5 SEM micrographs of a.) FG (as received) and b.) FG (washed).

d.) Differential thermal analysis (DTA)

DTA curves of FG and NG at a heating rate of 10°C/min in air and temperatures between 20-900°C were shown in Fig. 4.6

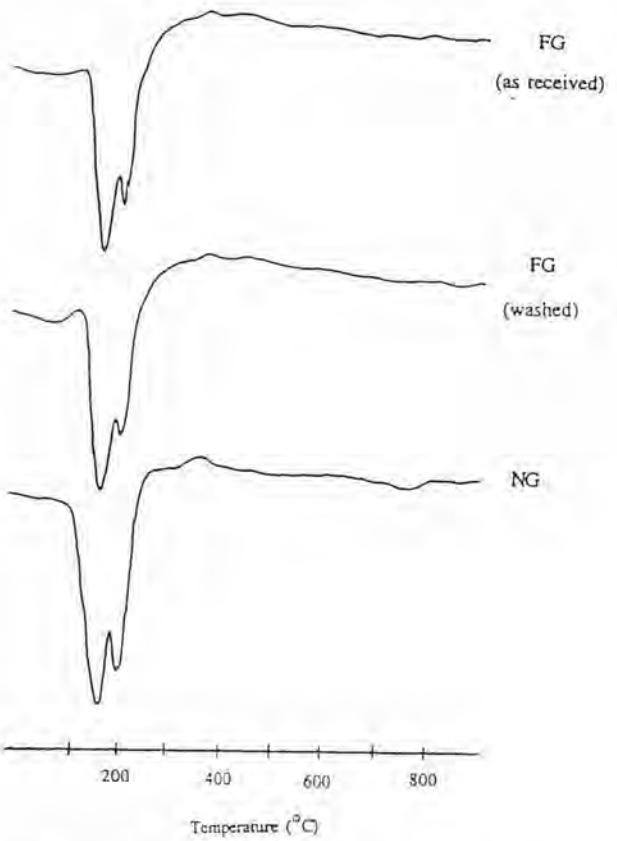

Fig. 4.6 DTA thermograms of FG and NG.

From the thermograms, FG (as received), FG (washed) and NG all showed two large endothermic peaks at 170°C and 200°C, corresponding to the loss of absorbed water and combined water. They were related to the formation of β-HH and γ-anhydrite which consisting of 1.5 and 1 moles of water, respectively. An exothermic peak at 380°C was referred to the transformation of γ-anhydrite to β-anhydrite or dead-burnt plaster. Especially, in NG an endothermic peak at 770°C was clearly observed. It was referred to the decomposition of the mineral phase in dolomite and the elimination of the carbonate.

4.2 Syntheses of β-HH and anhydrites

4.2.1 Phase analysis of β-HH and anhydrites

a.) Phase analysis of β-HH

XRD results of the phase composition of calcined FG and NG were presented in Fig. 4.7-4.8 and calculated results in Appendix : Table 2, page 150.

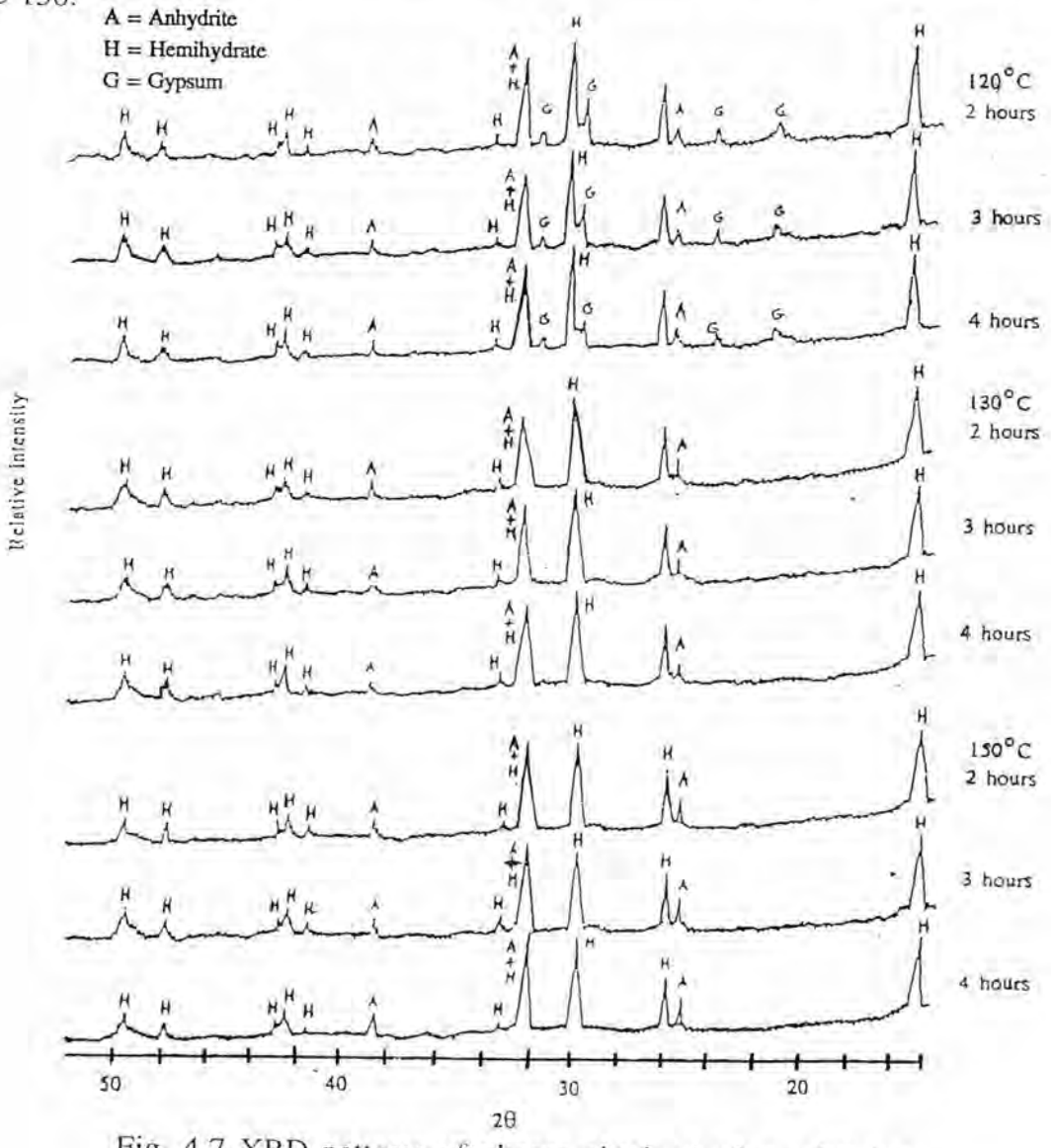

Fig. 4.7 XRD patterns of phases obtained after calcining the FG at 120-150°C for 2-4 hours.

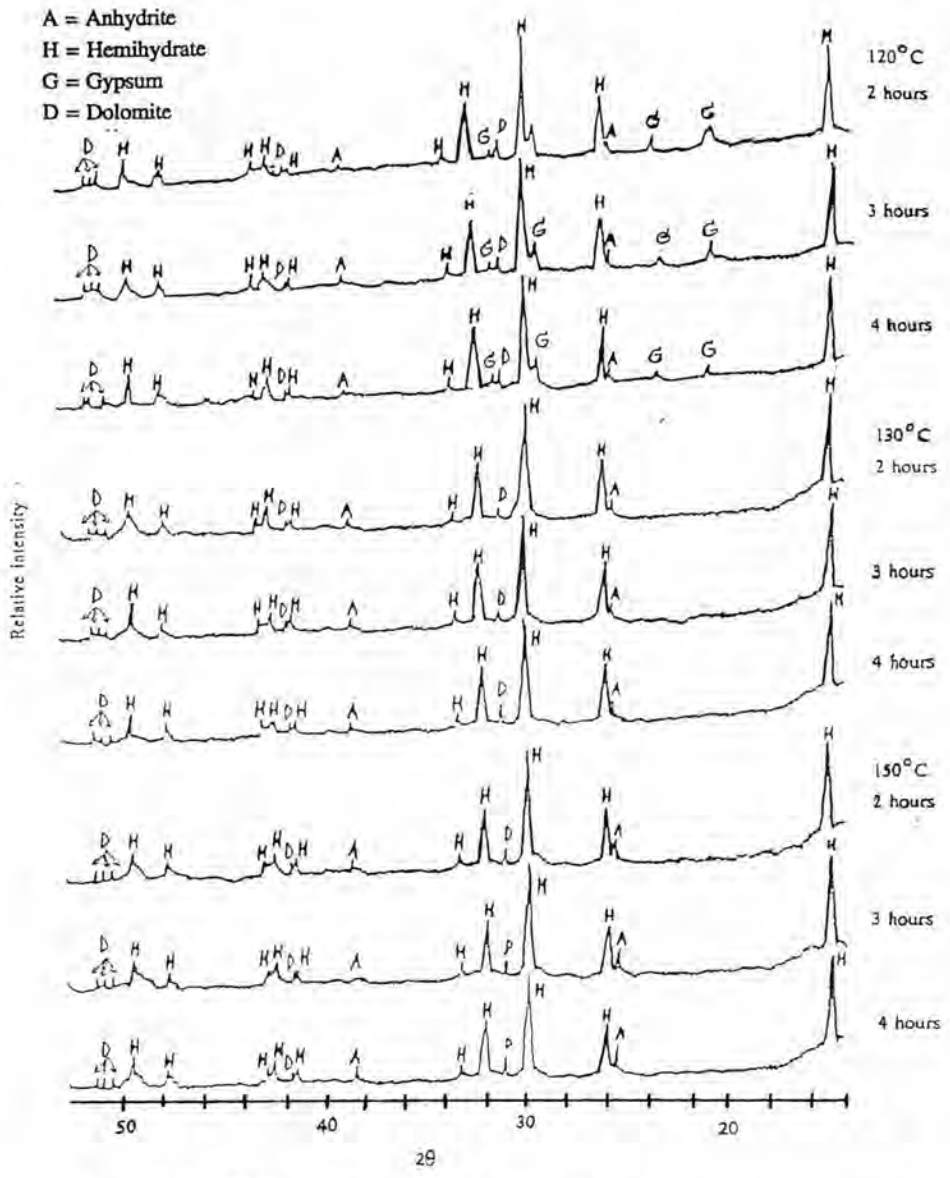

Fig. 4.8 XRD patterns of phases obtained after calcining the NG at 120-150°C for 2-4 hours.

The XRD analyses of both FG and NG calcined at 120°C showed the mixed phases of β-HH, anhydrite and DH because of the incomplete dehydration which was evident by the presence of the DH. At higher temperatures only β-HH and anhydrite were detected. Results in Appendix : Table 2 were the phase composition obtained by calculation. On the contrary, it was found from the calculation that DH was also present at 130 and 150°C but in a very little quantity and β-HH content increased with the temperature and time, maximum at 130°C, 4 hours and decreased when the calcination temperature reached 150°C.

b.) Phase analysis of anhydrite

The XRD results of anhydrite synthesized from FG and NG were shown in Fig. 4.9-4.10 and the calculated phase composition in Appendix : Table 3, page 151.

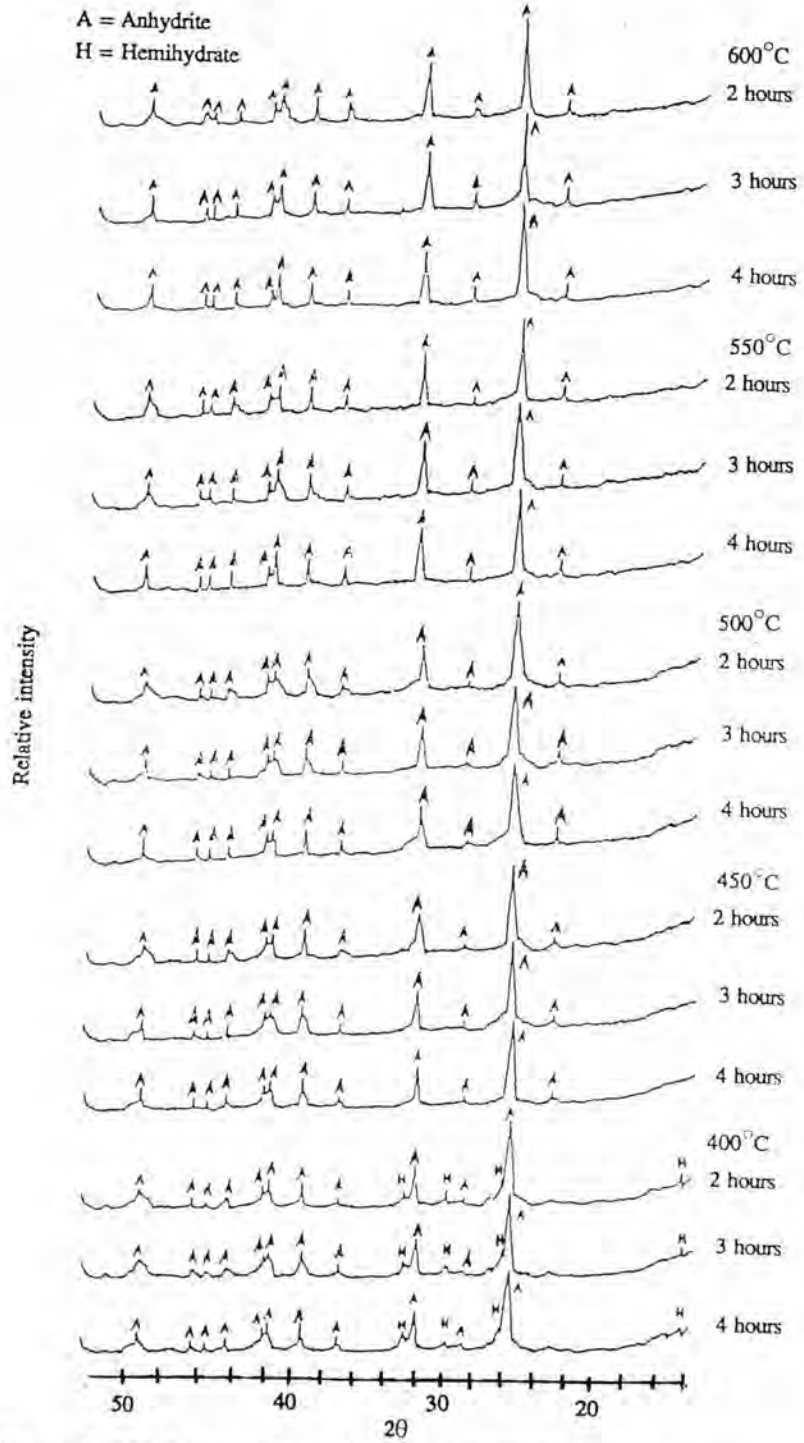

Fig. 4.9 XRD patterns of phases obtained after calcining the FG at 400-600°C for 2-4 hours.

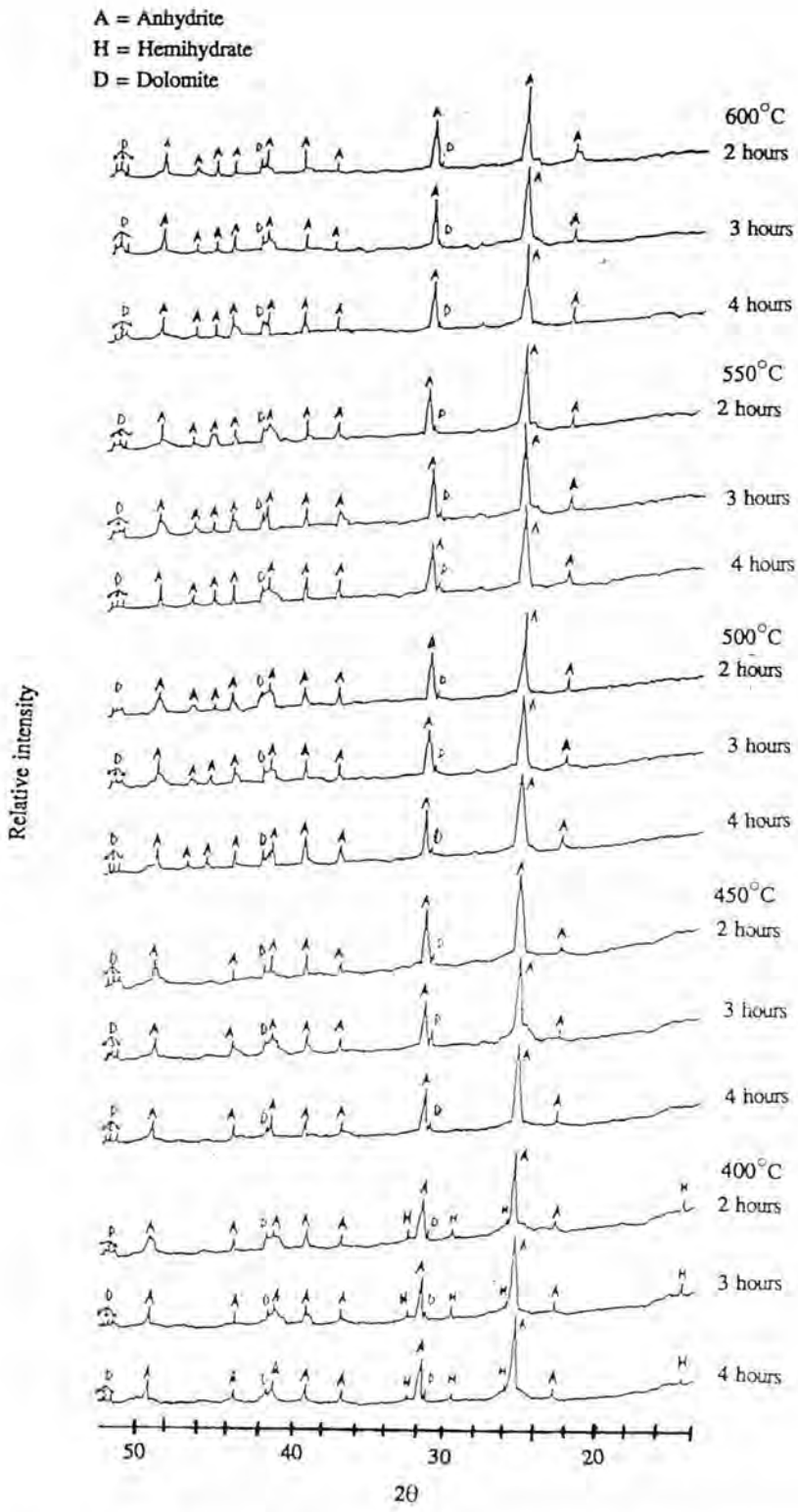

Fig. 4.10 XRD patterns of phases obtained after calcining the NG at 400-600°C for 2-4 hours.

The XRD patterns of anhydrite which was synthesized by calcining FG and NG at 400°C showed that anhydrite was the main phase and still some β-HH left but disappeared with increasing temperature. Appendix : Table 3 was the results of the calculated phase composition which revealed traces of β-HH upto 550°C, 3 hours for NG and 550°C, 4 hours for FG.

In conclusion, β-HH could be produced from FG and NG at temperatures 120-150°C. When calcining at 130°C for 4 hours, maximum amount of β-HH was obtained and the reproducibility was also better. However, DH was still present in very little quantity. This might be caused by the reaction of β-HH with water vapor in the air leading to the rehydration.

$$CaSO_4.1/2H_2O + 3/2H_2O \text{ ----------> } CaSO_4.2H_2O$$

When the calcining temperature was elevated from 400 to 600°C, anhydrite was formed along with small amount of β-HH because AIII might react readily with water vapor. But when the calcination temperature of FG and NG was raised to 600°C for 2 hours and 550°C for 4 hours, respectively, it was found from both the XRD results and the calculation that only anhydrite was formed.

Kuntze (1967) and Lehmann et al. (1973) reported that when calcined gypsums were stored, there was a change in their properties, called aging. This aging was caused by the uptake of water vapor from the air. Aridization method had been developed to avoid this phenomenon. According to what having been described, the condition of calcining FG and NG at 130°C for 4 hours was chosen for the aridization process (4.3).

4.2.2 Particle size distribution of β-HH and anhydrite

Particle sizes of β-HH and anhydrite from the calculation and the sieve analysis were shown in Appendix : Table 4-5, page 152 and Fig. 4.11, respectively.

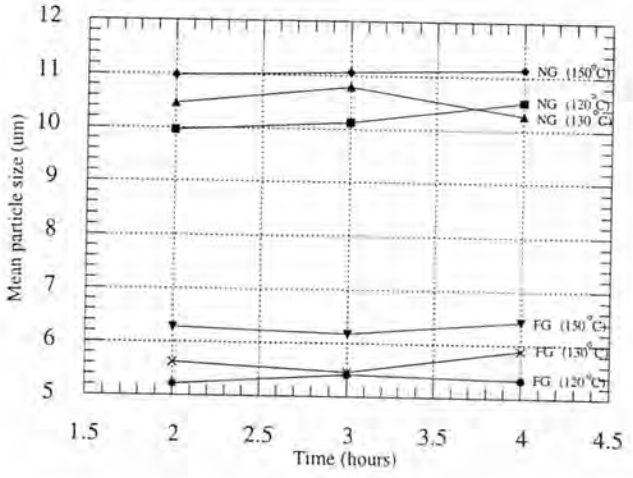

(a.)

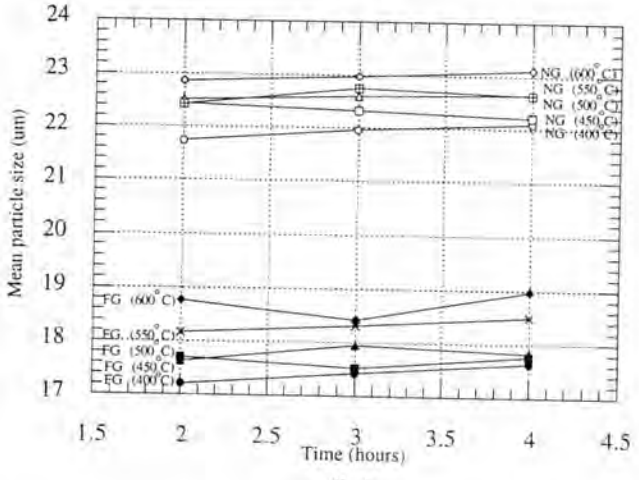

(b.)

Fig. 4.11 Particle size from the calculation of a.) β-HH and b.) anhydrite.

The results of Fig. 4.11 showed that particle sizes of β-HH and anhydrite increased with the increase of the calcination temperature and time. Further more β-HH and anhydrite might react with water vapor in air to change their phase and form agglomerates. So, they were ground and

sieved through 200 mesh screen to get rid of the agglomeration before use as starting meterials for the preparation of gypsum specimens.

4.2.3 DTA of β-HH and anhydrite

DTA results of β-HH and anhydrite were shown in Fig. 4.12. β-HH showed an endothermic peak at 200°C, corresponding to the loss of combined water and an exothermic peak at 380°C resulting from the conversion of γ-anhydrite to β-anhydrite. Anhydrite showed only the exothermic peak at 380°C, corresponding to phase transformation as for β-HH. Both β-HH and anhydrite that synthesized from NG also showed an additional endothermic peak at 770°C, corresponding to decomposition of mineral phases and carbonate of dolomite.

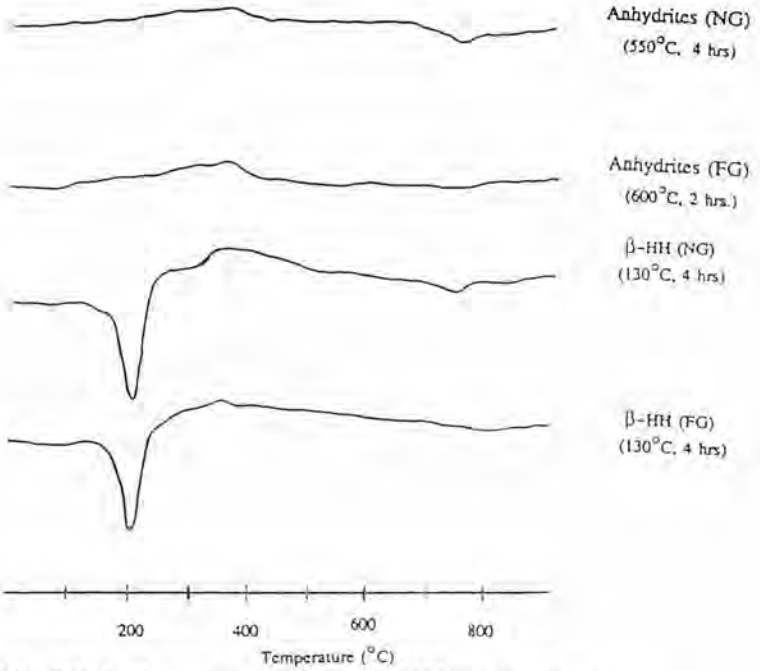

Fig. 4.12 DTA thermograms of β-HH and anhydrite.

4.3 Effect of aridization on β-HH and anhydrite

Results of the aridization of β-HH and anhydrite were shown in Fig. 4.13-4.14 and Appendix : Table 6, page 153.

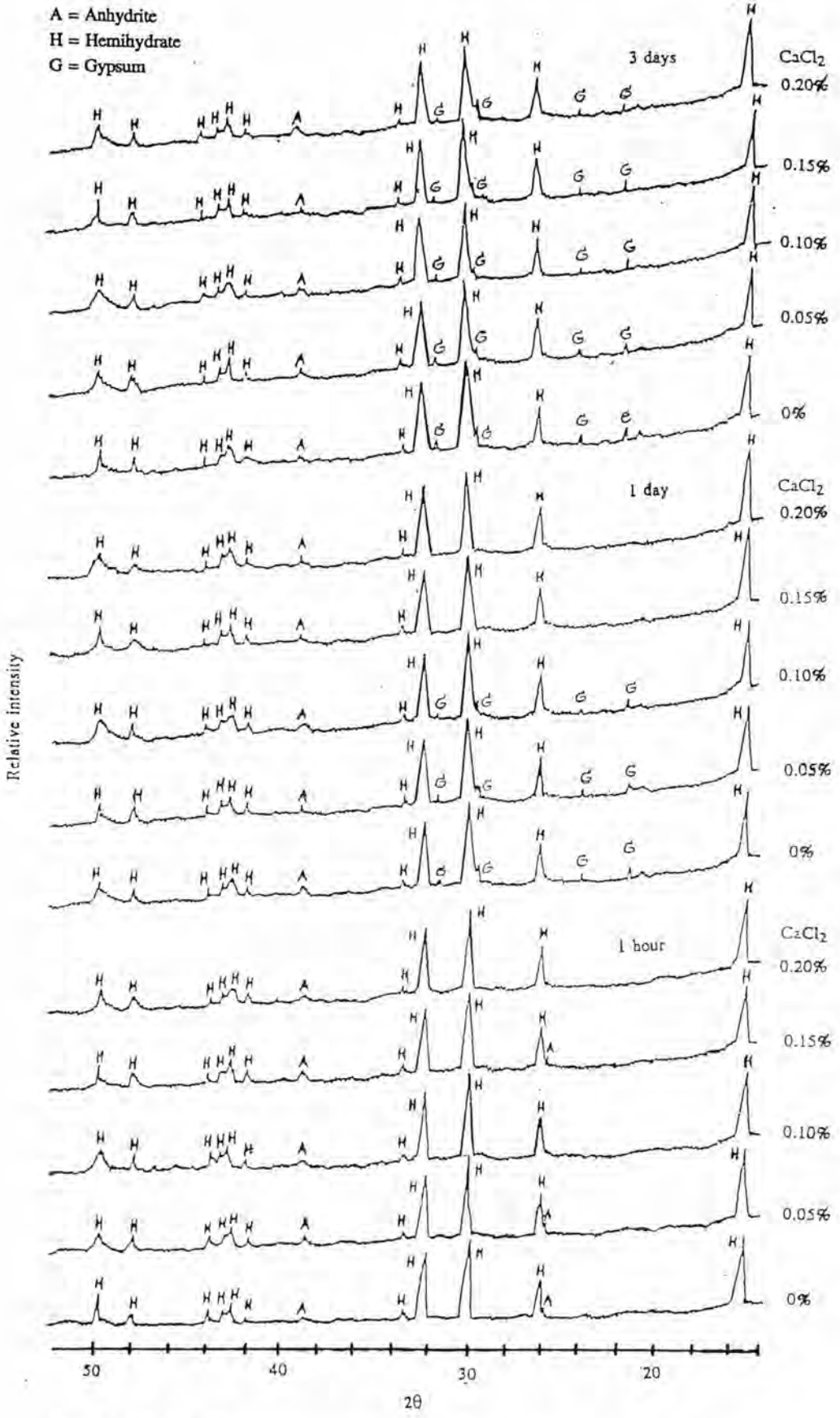

Fig. 4.13 XRD patterns of phases obtained after exposing β-HH (FG) with various amounts of $CaCl_2$ to air.

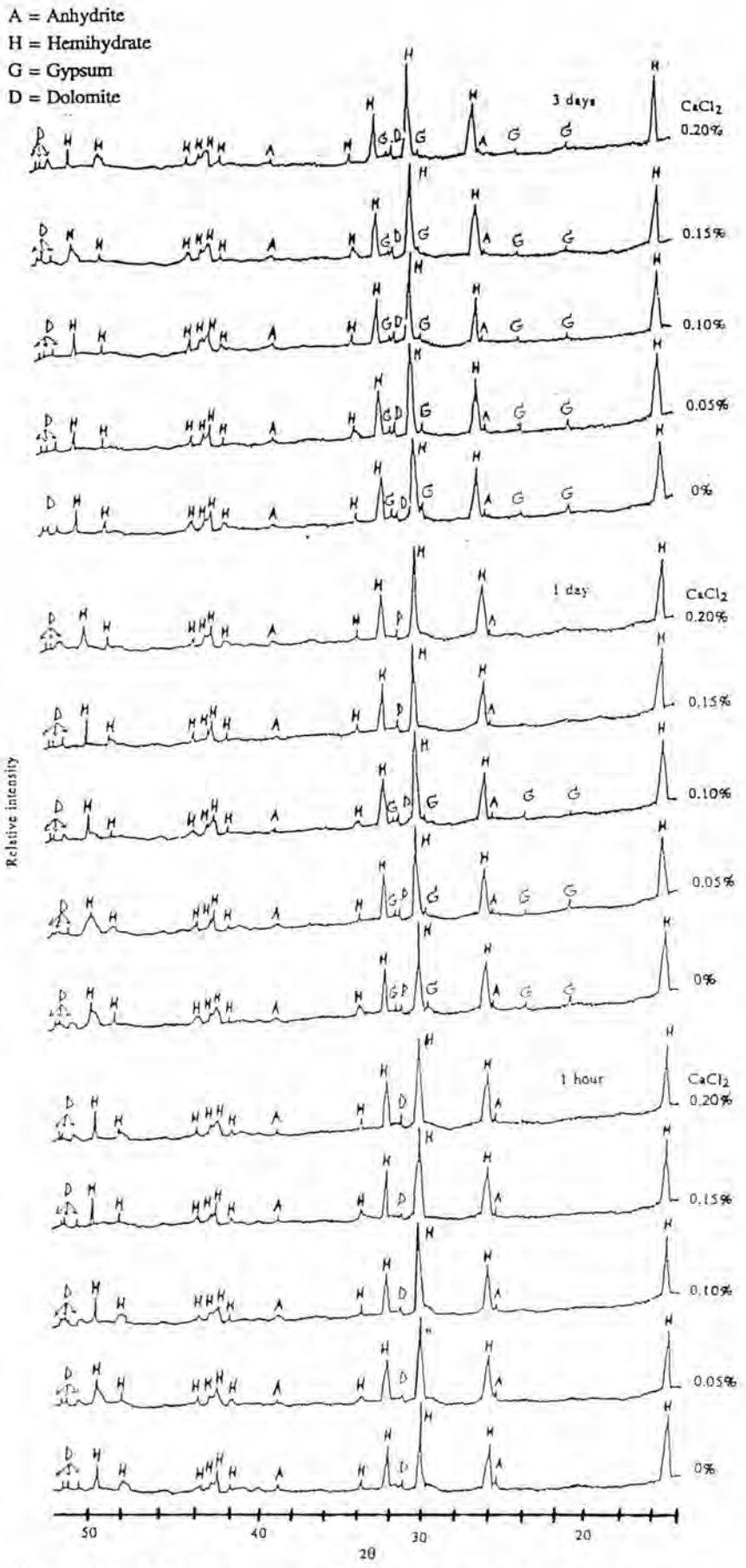

Fig. 4.14 XRD patterns of phases obtained after exposing β-HH (NG) with various amounts of $CaCl_2$ to air.

XRD patterns of Fig. 4.13 and 4.14 revealed that addition of $CaCl_2$ could decrease the formation of DH in the β-HH from both FG and NG when exposed to air. Also the results from Appendix : Table 6 confirmed that the content of DH decreased with increasing $CaCl_2$ content. This might be caused by the rapid reaction of $CaCl_2$ with water vapor in air to form $Ca(OH)_2$ and HCl prior to DH because $CaCl_2$ was more active than β-HH.

$$CaCl_2 + 2H_2O \text{ ----------> } Ca(OH)_2 + 2HCl$$

So, $CaCl_2$ could prevent the rehydration of β-HH to DH but HCl which was the by-product of the reaction acted as the accelerator, hence affected the setting time of β-HH (Fig. 4.15).

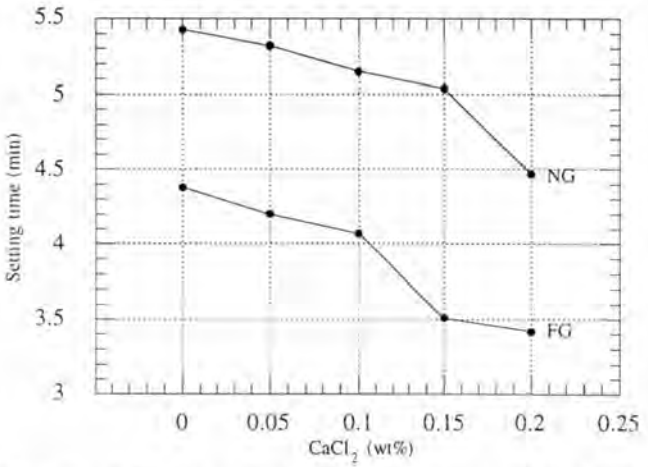

Fig. 4.15 Effect of $CaCl_2$ on the setting time of β-HH (W/P = 0.9).

From Fig. 4.15, it was indicated that the setting time decreased with the increase of the content of $CaCl_2$. So, the minimum amount of $CaCl_2$ that could prevent the rehydration was chosen as 0.15% and 0.10% for β-HH that synthesized from FG and NG, respectively and this amount of $CaCl_2$ was also chosen to aridize the anhydrite. Hence the reproduction of β-HH and anhydrite with addition of $CaCl_2$ as aridizing agent was shown in Appendix : Table 7, page 153 and Fig. 4.16.

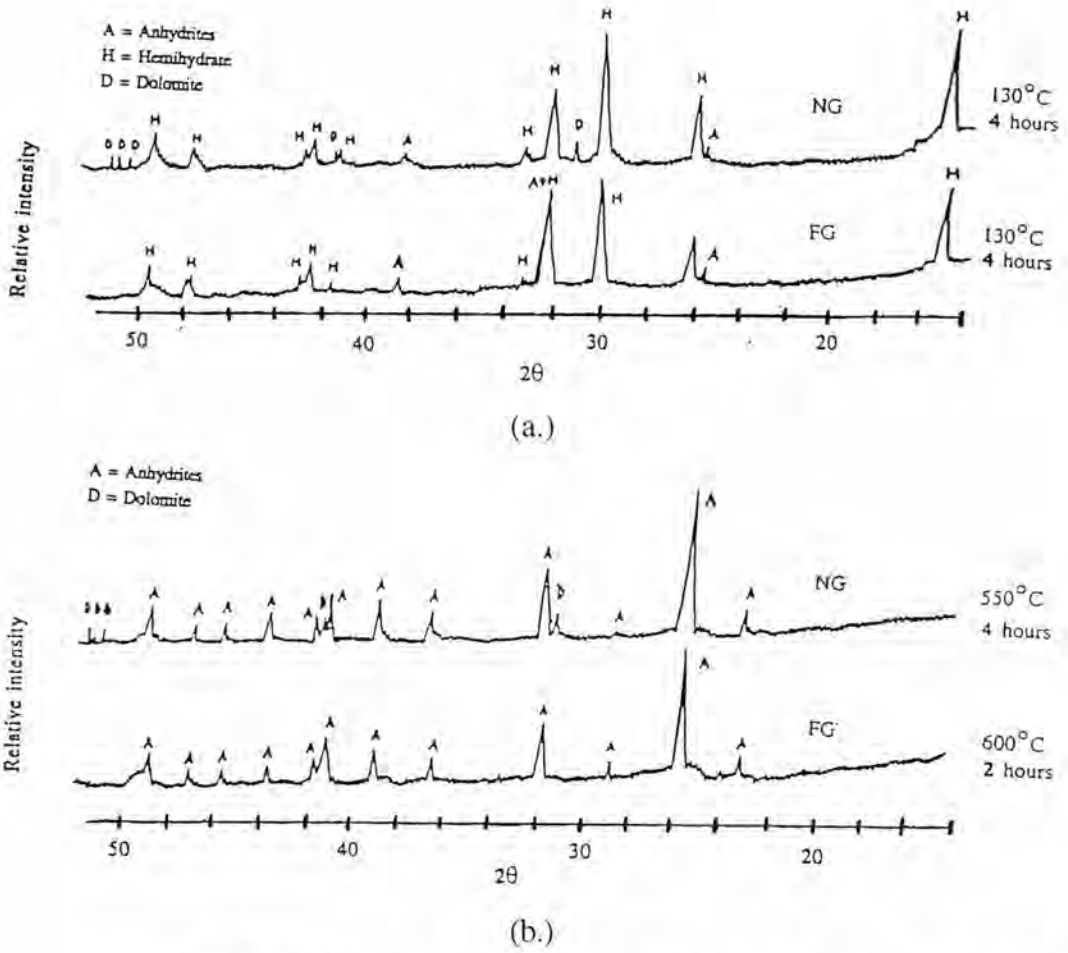

Fig. 4.16 XRD patterns of phases obtained after reproducing a.) β-HH and b.) anhydrite.

Results from the Appendix : Table 7 and Fig. 4.16 revealed no trace of DH, so they confirmed the reproducibility of previous finding.

4.4 Preparation of MP

4.4.1 Effect of agglomeration of FG

a.) Physical properties of FG briquet and pellet

Physical properties of B and P were shown in Table 4.2 and Fig. 4.17.

Table 4.2 Physical properties of B and P.

Compaction pressure (bars)	Load/Area (kg/cm^2)	Apparent density (g/cm^3)		Max. load (N)	
		B	P	B	P
50	196	1.65±0.03	1.32±0.04	405.23±3.05	293.37±2.76
100	392	1.71±0.04	1.49±0.04	432.78±2.78	331.90±3.18
150	588	1.89±0.05	1.53±0.05	476.50±2.46	386.54±2.54
200	784	2.10±0.05	1.68±0.06	515.81±2.90	421.41±3.02

* the number of each sample specimens was 5.

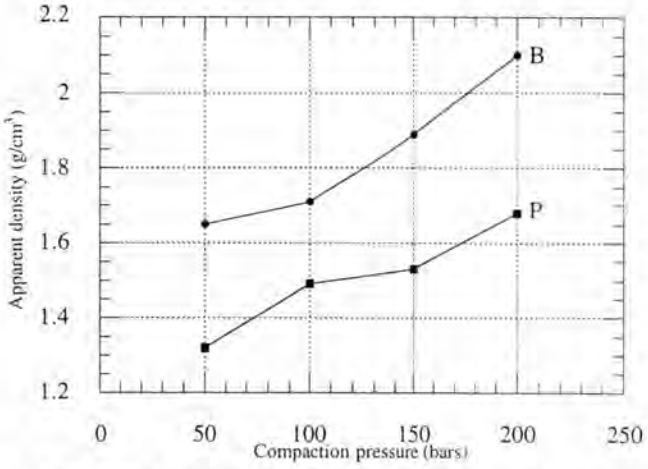

Fig. 4.17 Effect of compaction pressure on the apparent densities of B and P.

Table 4.2 and Fig. 4.17 showed that apparent densities of B and P increased with the increase of compaction pressure. Wirsching (1984) reported the apparent densities of B and P were 2.15 and 1.60 g/cm^3 respectively and unfavorable size and shape of FG particles were eliminated by compaction under high pressure to form solid structure.

According to what having been described, compaction of B and P at 200 bars corresponding to apparent density of 2.10 and 1.68 g/cm^3 was chosen to produce MP after their persistent particle morphology had been investigated by SEM.

b.) Particle morphology

Scanning electron micrographs of B and P were shown in Fig. 4.18. It was found from B and P compacted at a compaction pressure 100 bars that initial morphology of FG crystal was still present as rod shape and when the compaction pressure increased to 200 bars the original rod shaped crystal of FG was eliminated by intergrowing into a rocklike body.

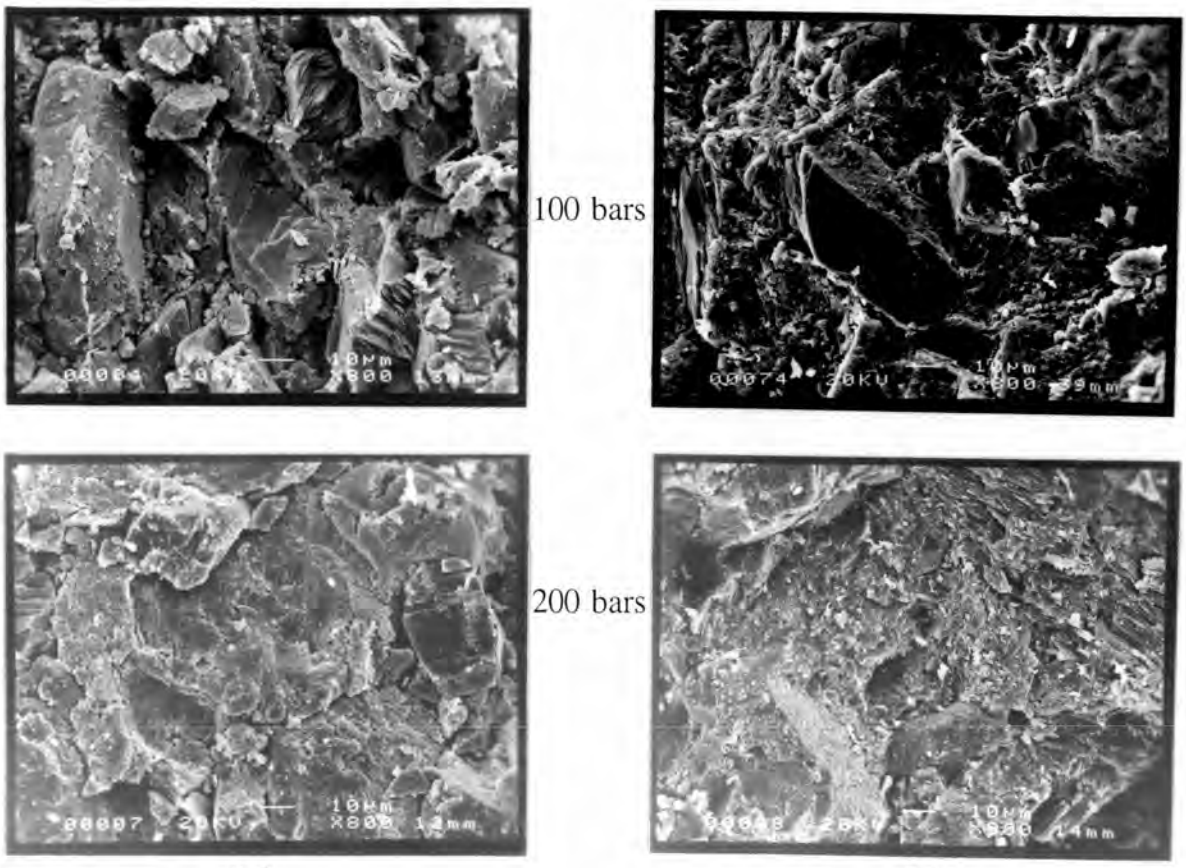

Fig. 4.18 SEM micrographs of compacted FG with compaction pressures of 100 bars and 200 bars. a.) B and b.) P.

4.4.2 Phase analysis of MP.

Results of phase analysis of MP were illustrated and tabulated in Fig. 4.19–4.22 and Appendix : Table 8, page 154.

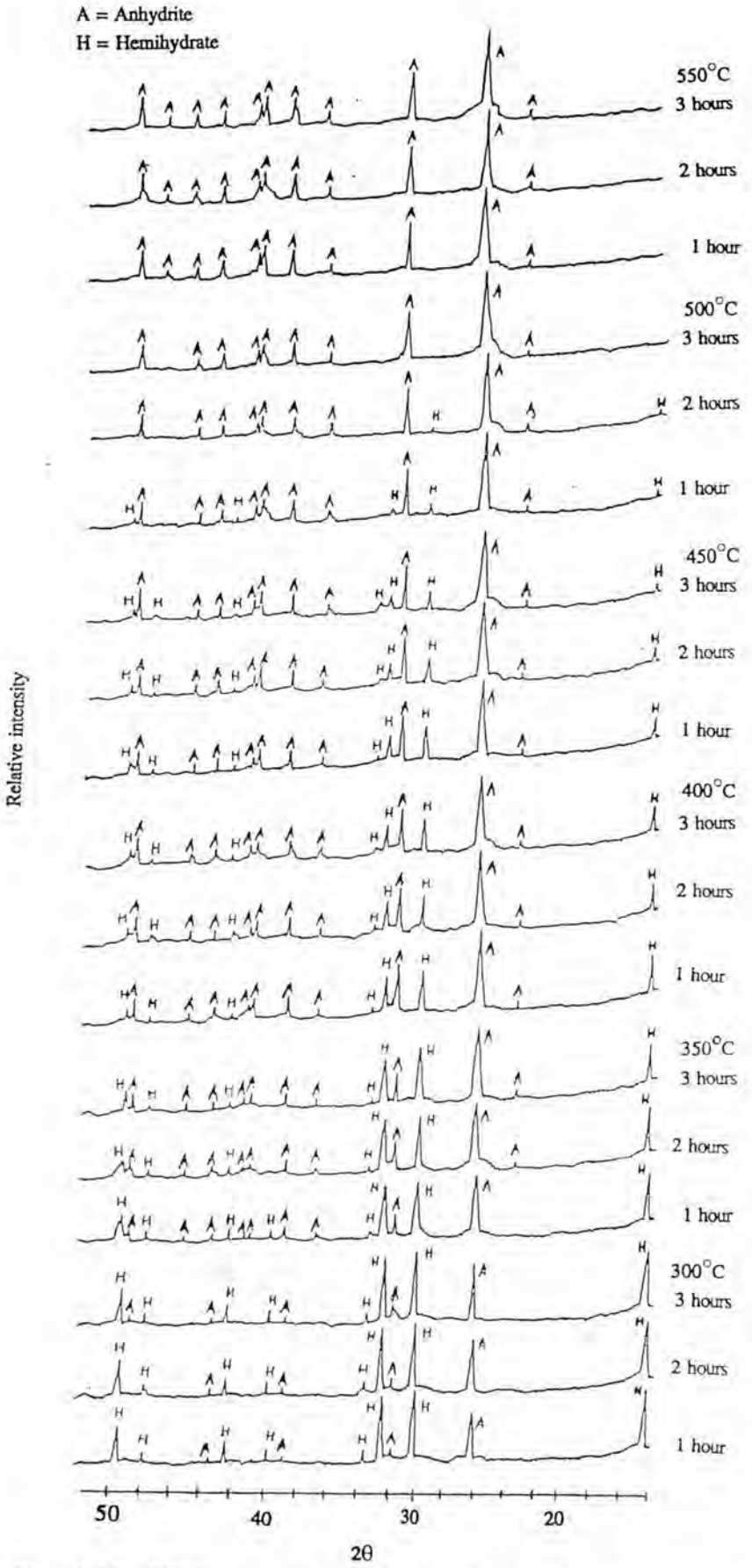

Fig. 4.19 XRD patterns of phases obtained after calcining B (50x50x5 mm.) at 300-550°C for 1-3 hours.

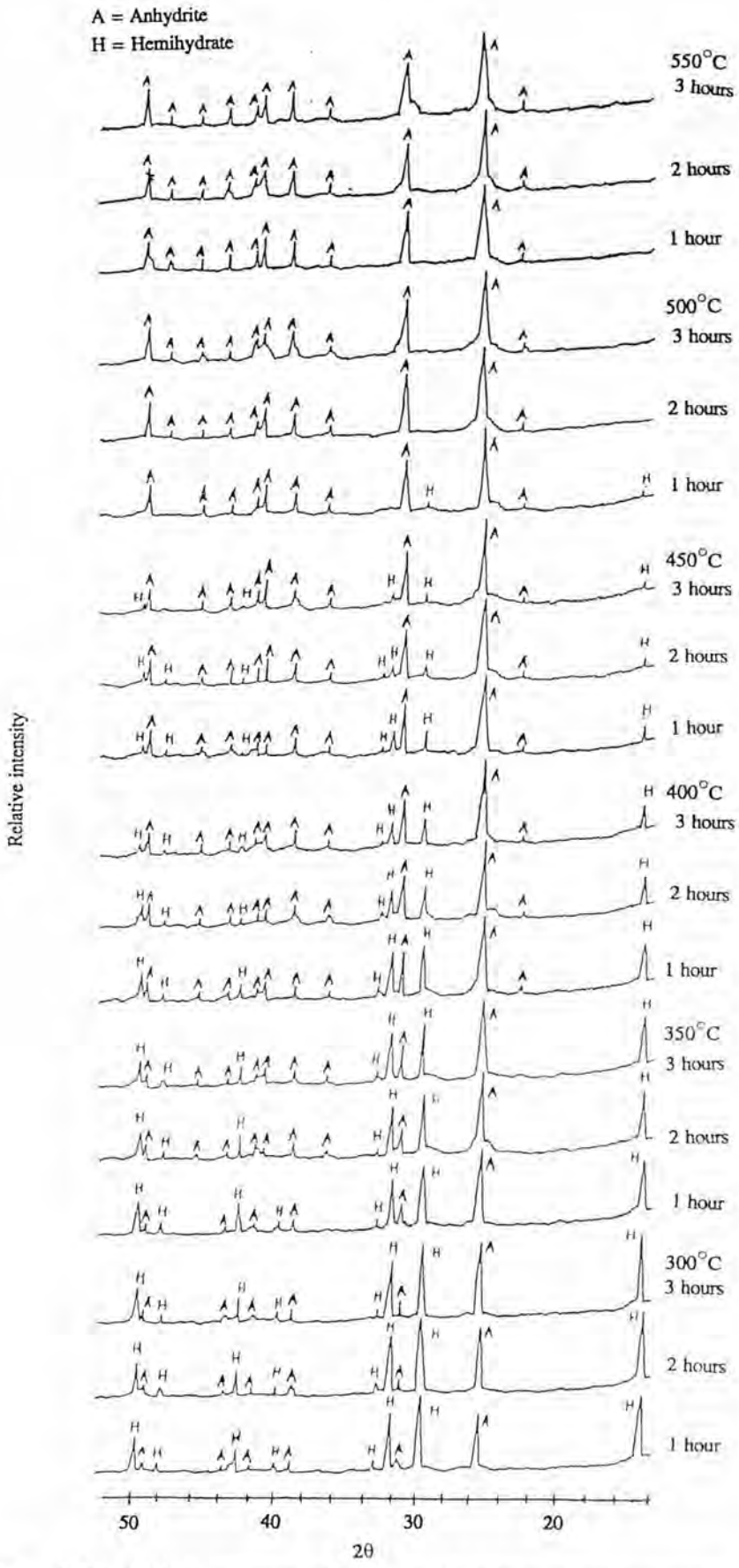

Fig. 4.20 XRD patterns of phases obtained after calcining P (50x50x5 mm.) at 300–550°C for 1–3 hours.

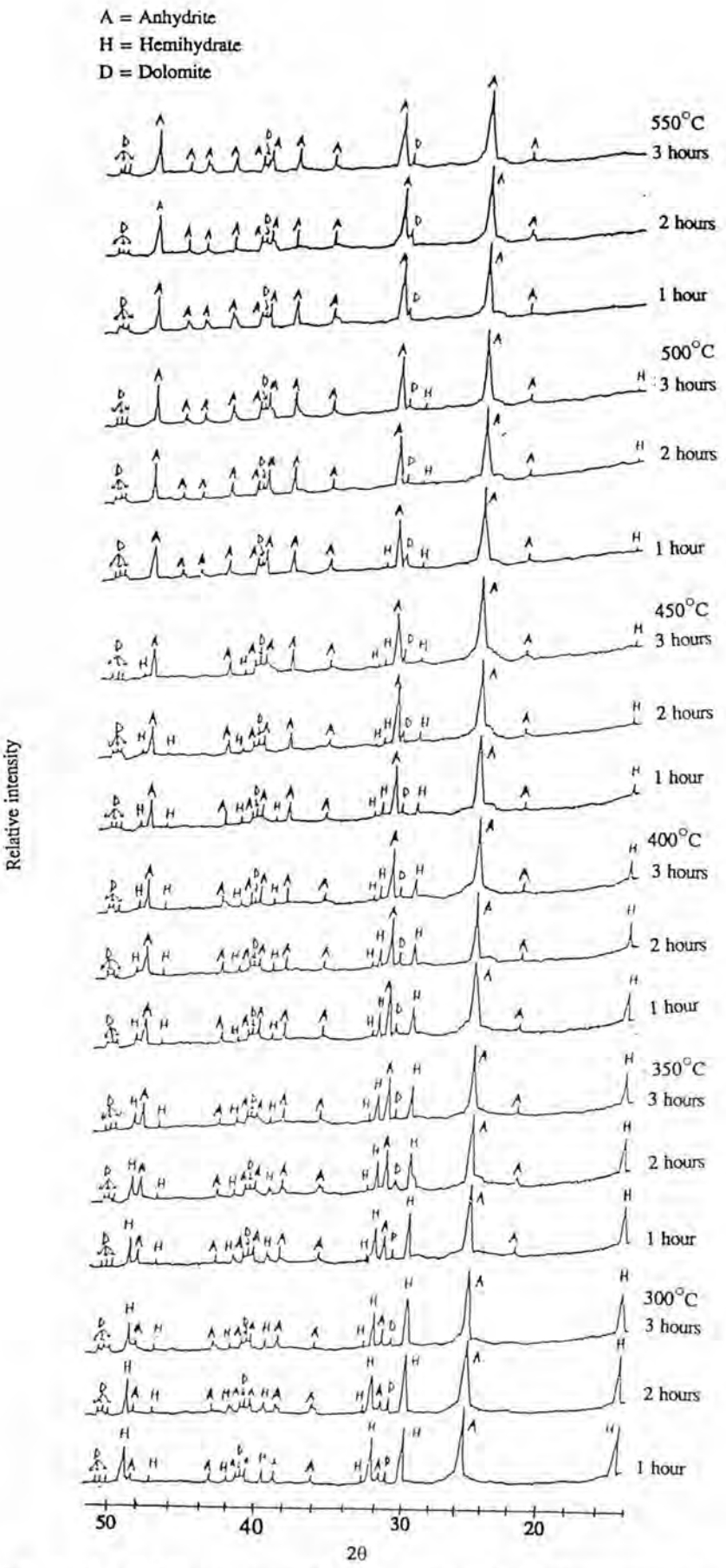

Fig. 4.21 XRD patterns of phases obtained after calcining NG (2.36–3.35 mm.) at 300–550°C for 1–3 hours.

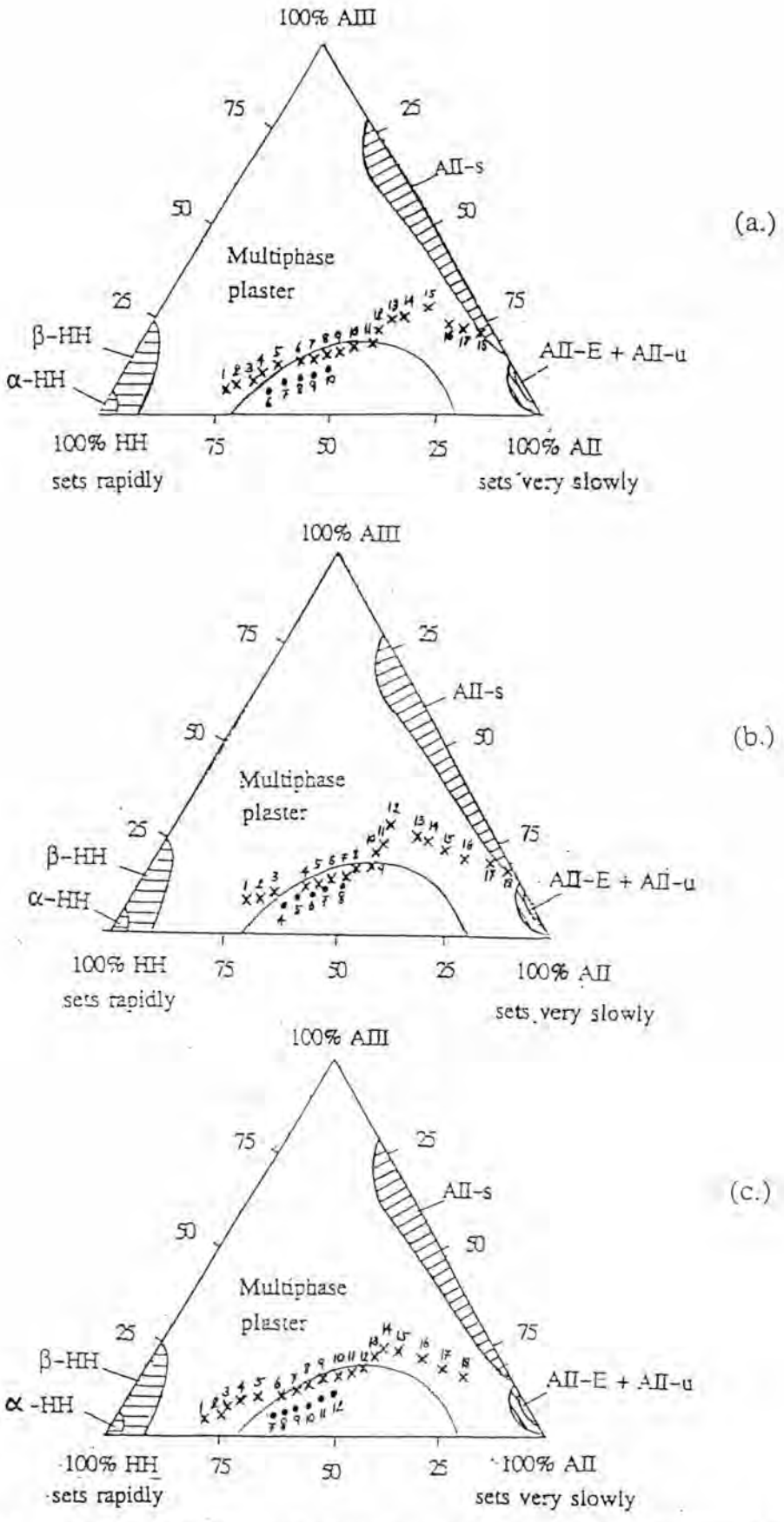

Fig. 4.22 Relationship of three phase compositions of MP prepared from a.) B, b.) P and c.) NG (× B, P was 50x50x5 mm., NG was 2.36–3.35 mm. and • B, P was 50x50x10 mm., NG was 4.75–5.60 mm.)

The XRD patterns of MP which prepared from B, P and NG were shown in Fig. 4.19-4.21. It was found from 300°C to higher temperatures that the mixture between anhydrite and β-HH was always present and β-HH content decreased with temperature and disappeared above 500°C. Fig. 4.22 was the plots of phase composition of MP which obtained from the calculation (Appendix : Table 8). It was found from the plot that some of calcining conditions could produce MP because they consisted of phase compositions in the MP range but these compositions were too close to the boundary of MP phase field. So, B, P and NG with increase in size were used to adjust the phase composition of MP. The results were shown in Fig. 4.23-4.24 and Appendix : Table 9, page 155.

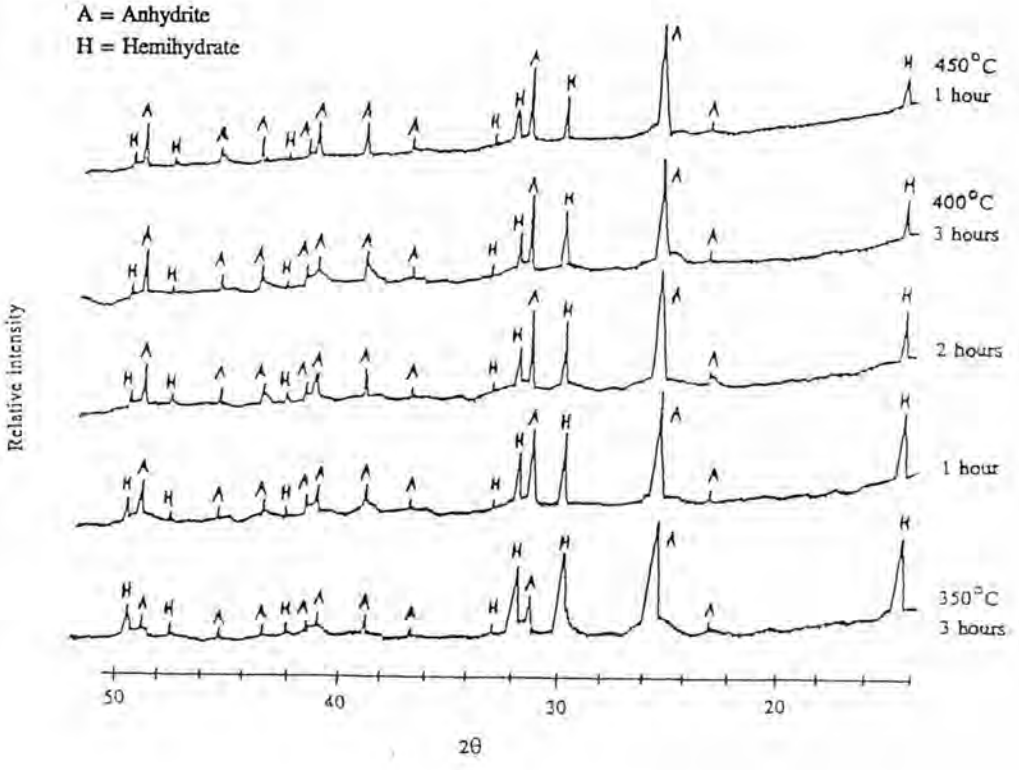

Fig. 4.23 XRD patterns of phases obtained after calcining B (50x50x10 mm.).

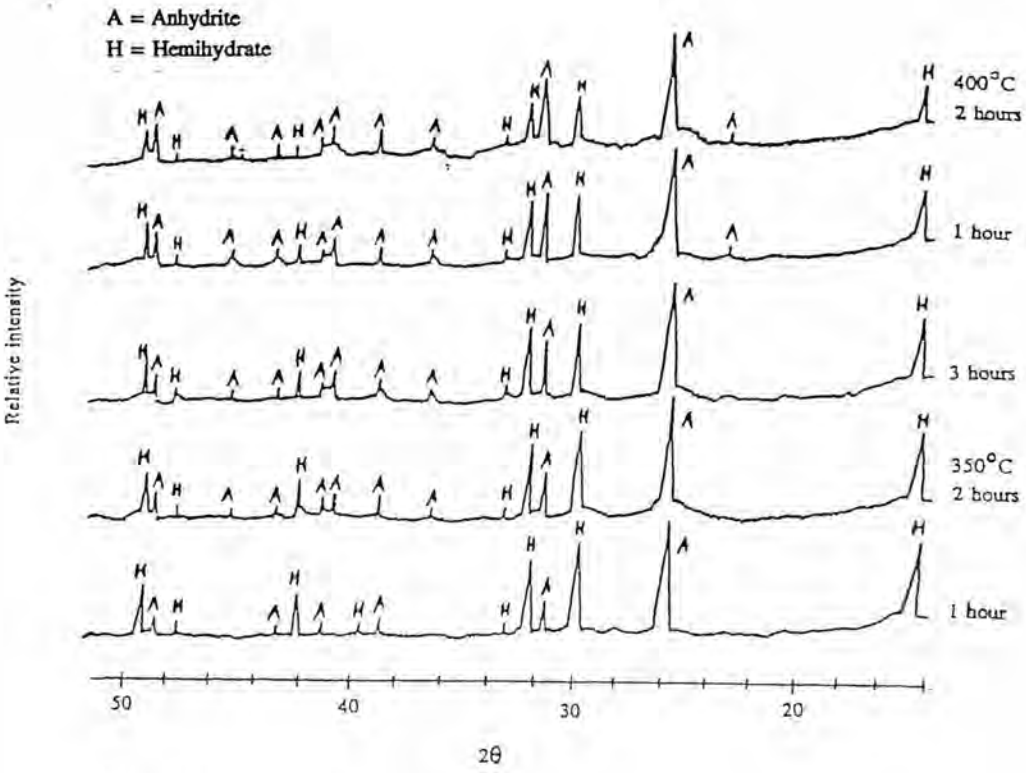

Fig. 4.24 XRD patterns of phases obtained after calcining P (50x50x10 mm.).

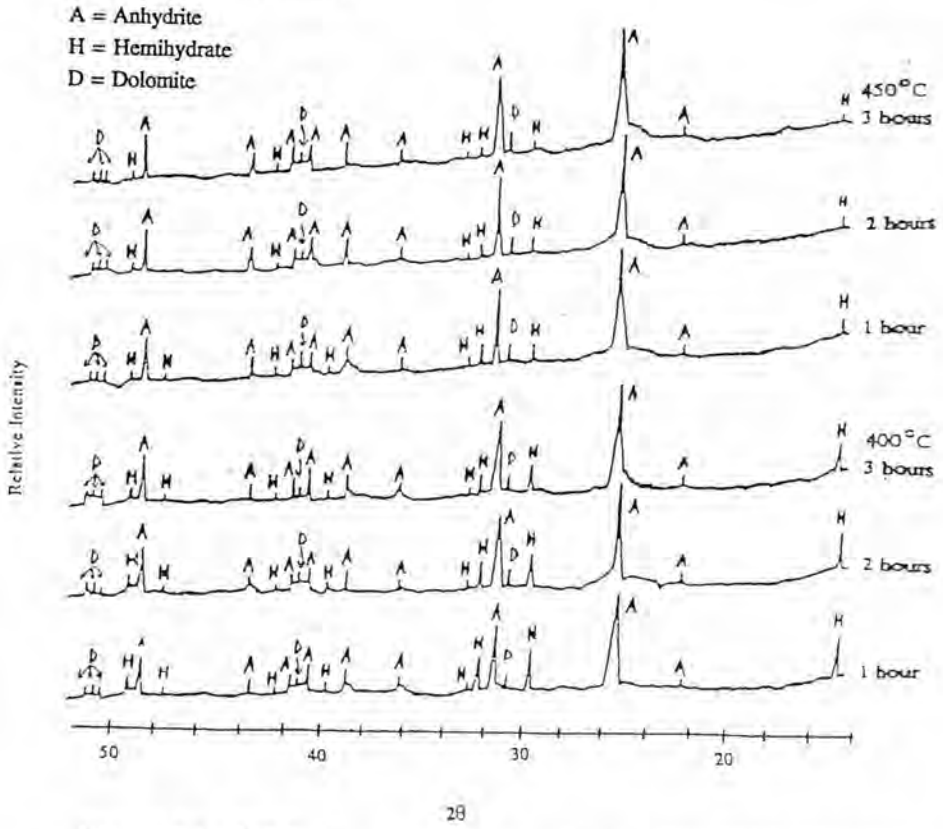

Fig. 4.25 XRD patterns of phases obtained after calcining NG (4.75–5.60 mm.).

Results from Fig. 4.23-4.25 and Appendix : Table 9 indicated the presence of mixed phases between anhydrite and β-HH. The plots of phase composition were also shown in Fig. 4.22. It was found from the plots that all of the phase compositions were in MP range and well inside the MP phase field. It was obvious that the increase in size of B, P and NG resulted in the increase in temperature gradient between the surface and the inside of them which was evident by the presence of higher content of β-HH.

4.4.3 DTA of MP

Thermograms of MP were shown in Fig. 4.26. They showed an endothermic peak at 200°C and an exothermic peak at 380°C which were referred to loss of combined water of β-HH and the transformation of γ-anhydrite to β-anhydrite, respectively. For MP that synthesized from NG, again, showed an endothermic peak at 770°C, corresponding to the decomposition of mineral phase and carbonate of dolomite.

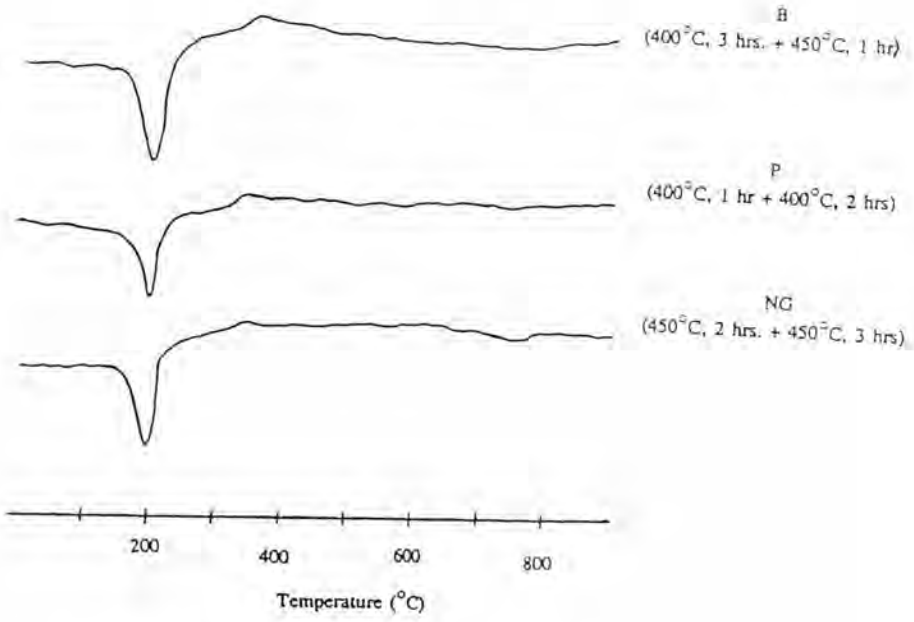

Fig. 4.26 DTA thermograms of MP.

4.5 Preparartion of gypsum board specimen from β-HH and MP

4.5.1 Setting time of gypsum specimens

a) Preparation of gypsum specimens from β-HH

The effect of various additives as retarder on setting time of β-HH powder was Tabulated and illustrated in Table 4.3-4.7 and Fig. 4.27-4.31.

Table 4.3 Effect of content of citric acid on setting time of β-HH (humidity = 64%, room and water temperatures = 20°C and 25°C, pH of water = 7.35 and W/P = 0.9).

Citric acid (wt%)	Flowability		Setting time (min.)			
			Initial		Final	
	FG	NG	FG	NG	FG	NG
0.00	good	good	4.07	5.26	7.45	6.30
0.02	good	good	6.23	7.59	9.36	8.45
0.04	good	good	8.46	10.02	12.54	11.09
0.06	good	good	11.17	13.41	15.01	14.26
0.08	good	good	15.44	19.38	21.24	20.20
0.10	good	good	21.37	26.42	28.50	27.35

* the number of test sample was 3 (DIN 1168).

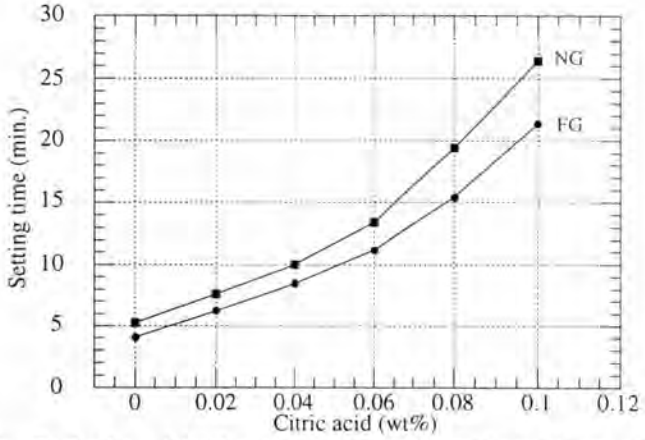

Fig. 4.27 Relationship between initial setting time of β-HH and the content of citric acid (W/P = 0.9).

Table 4.4 Effect of content of methycellulose on setting time of β-HH (humidity = 67%, room and water temperatures = 21°C and 25°C, pH of water = 7.26, W/P = 0.9).

Methyl cellulose (wt%)	Flowability		Setting time (min.)			
			Initial		Final	
	FG	NG	FG	NG	FG	NG
0.00	good	good	4.13	5.31	7.25	6.10
0.02	good	good	6.07	7.14	9.40	8.29
0.04	good	good	8.35	9.38	11.15	10.26
0.06	good	good	10.27	13.15	15.02	14.10
0.08	good	good	13.48	16.27	18.59	17.38
0.10	good	good	15.22	19.45	21.53	20.36

* the number of test sample was 3 (DIN 1168).

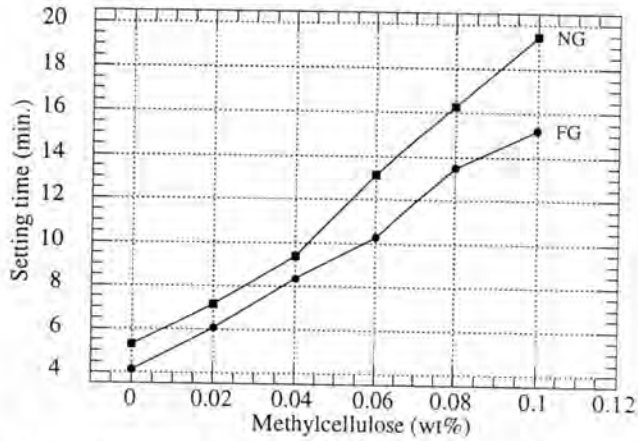

Fig. 4.28 Relationship between initial setting time of β-HH and the content of methycellulose (W/P = 0.9).

Table 4.5 Effect of content of acetic acid on setting time of β-HH (humidity = 72%, room and water temperatures = 19°C and 25°C, pH of water = 7.02, W/P = 0.9).

Acetic acid (wt%)	Flowability		Setting time (min.)			
			Initial		Final	
	FG	NG	FG	NG	FG	NG
0.00	good	good	4.18	5.40	7.55	6.22
0.20	good	good	5.43	6.13	8.26	7.04
0.40	good	good	7.36	8.35	10.30	9.50
0.60	good	good	8.25	10.45	12.50	11.39
0.80	good	good	10.37	13.57	15.26	14.38
1.00	good	good	11.54	16.36	18.30	17.21

* the number of test sample was 3 (DIN 1168).

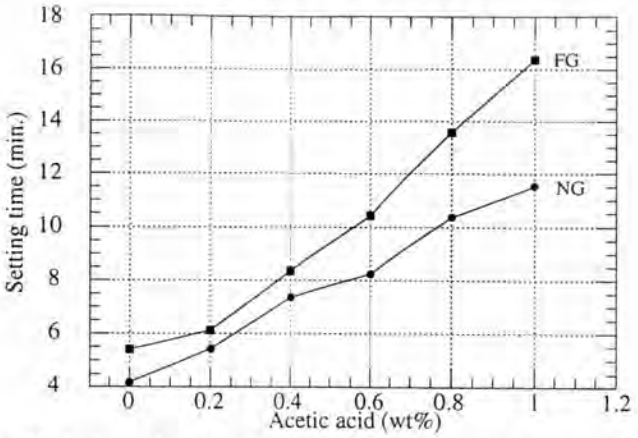

Fig. 4.29 Relationship between initial setting time of β-HH and the content of acetic acid (W/P = 0.9).

Table 4.6 Effect of content of potassium alum on setting time of β-HH (humidity = 66%, room and water temperatures = 20°C and 26°C, pH of water = 7.52 and W/P = 0.9).

Potassium alum (wt%)	Flowability		Setting time (min.)			
			Initial		Final	
	FG	NG	FG	NG	FG	NG
0.00	good	good	4.15	5.37	7.11	6.21
0.20	good	good	5.46	7.10	9.55	8.36
0.40	good	good	7.38	8.56	10.50	9.31
0.60	good	good	8.21	11.21	12.59	12.36
0.80	good	good	10.49	14.47	16.21	15.40
1.00	good	good	12.38	16.55	18.31	17.26

* the number of test sample was 3 (DIN 1168).

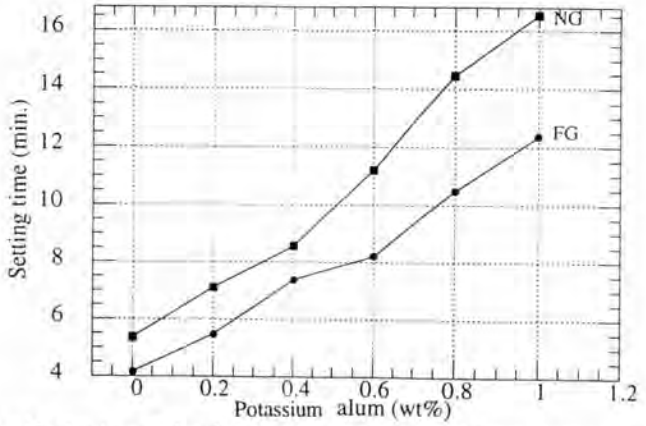

Fig. 4.30 Relationship between initial setting time of β-HH and the content of potassium alum (W/P = 0.9).

Table 4.7 Effect of content of sodium borate on setting time of β-HH (humidity = 70%, room and water temperatures = 21°C and 25°C, pH of water = 7.14 and W/P = 0.9).

Sodium borate (wt%)	Flowability		Setting time (min.)			
			Initial		Final	
	FG	NG	FG	NG	FG	NG
0.00	good	good	4.20	5.45	7.41	6.20
0.20	good	good	5.51	6.15	8.20	7.24
0.40	good	good	7.16	8.30	10.37	9.26
0.60	good	good	8.57	12.50	14.40	13.32
0.80	good	good	10.34	16.24	17.14	16.48
1.00	good	good	12.12	18.33	19.50	19.24

* the number of test sample was 3 (DIN 1168).

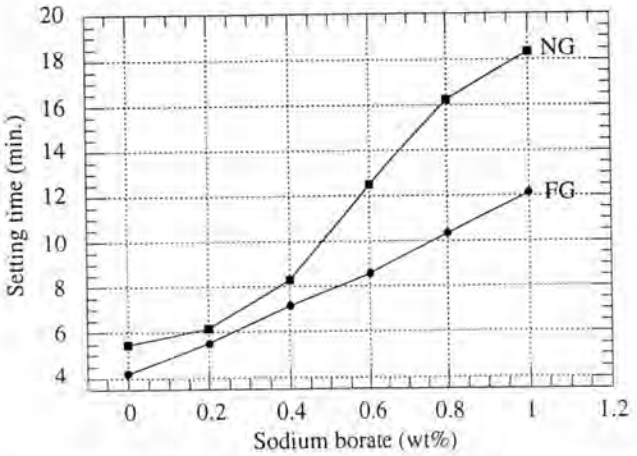

Fig. 4.31 Relationship between initial setting time of β-HH and the content of sodium borate (W/P = 0.9).

Fig. 4.27-4.31 were the plots between wt% of additive and initial setting time (min) of β-HH. It was found from the plots that initial setting time of β-HH could be controlled to meet requirement for gypsum board (5-8 min) by adjusting the content of additive and they also showed that the setting time of β-HH increased with the content of additive. Among the additives used, citric acid and methylcellulose were better retarders because with the same content they gave a longer initial setting time.

Results of Table 4.8 confirmed the reproducibility in obtaining the required setting time for gypsum board specimen by using suitable contents of retarder.

Table 4.8 Setting time of gypsum board specimens containing the mixture of β-HH and suitable amount of additives as retarder (humidity = 66%, room and water temperatures = 21°C and 25°C, pH of water = 7.10, W/P = 0.9).

Additives	Content (wt%)		Setting time (min.)			
			Initial		Final	
	FG	NG	FG	NG	FG	NG
None	-	-	4.28±0.30	5.51±0.35	7.56±0.38	6.36±0.26
Citric acid	0.02	0.02	6.49±0.36	8.35±0.40	10.11±0.25	9.41±0.35
	0.04	-	8.57±0.28	-	13.20±0.39	-
Methylcellulose	0.02	0.02	6.24±0.41	8.11±0.31	9.45±0.35	9.16±0.27
	0.04	-	8.18±0.35	-	11.26±0.40	-
Acetic acid	0.20	0.20	5.56±0.40	6.21±0.29	8.38±0.30	7.13±0.24
	0.40	0.40	7.42±0.25	8.51±0.35	10.45±0.29	9.55±0.30
Potassium alum	0.20	0.20	5.50±0.20	6.17±0.37	8.16±0.27	8.40±0.21
	0.40	0.40	7.31±0.31	8.44±0.26	10.24±0.20	9.36±0.41
Sodium borate	0.20	0.20	6.10±0.31	6.21±0.20	9.30±0.38	7.33±0.28
	0.40	0.40	7.54±0.34	8.48±0.39	11.12±0.41	9.39±0.32

* repeat with 5 tests in each composition.

Kuhlmann and Ludwig (1977) reported that the additives induced a change in structure so that the strength was change. An obvious example of reducing strength was the effect of citric acid, the increasing citric acid addition resulted in the increase of setting retardation and the time between initial and final sets became broader but strong decrease in strength. According to what described above, the particle morphology and flexural strength of β-HH added with additives should be investigated.

b) Preparation of gypsum board specimens from MP

The effect of additives as accelerator on setting time of MP was tabulated and illustrated in Table 4.9-4.11 and Fig. 4.32-4.34.

Table 4.9 Effect of content of calcium sulfate dihydrate on setting time of MP (humidity = 77%, room and water temperatures = 20°C and 25°C, pH of water = 7.29, W/P = 0.9)

Calcium sulfate dihydrate (wt%)	Flowability			Setting time (min.)					
				Initial			Final		
	B	P	NG	B	P	NG	B	P	NG
0.00	good	good	good	25.39	27.02	30.15	64.26	72.44	44.36
0.50	good	good	good	18.58	19.46	24.40	52.17	59.30	35.15
1.00	good	good	good	11.20	13.35	19.52	40.47	47.17	28.20
1.50	medium	medium	good	6.12	6.35	12.36	28.38	36.29	15.33
2.00	poor	poor	medium	2.01	3.58	7.14	22.50	30.53	11.45

* the number of test sample was 3 (DIN 1168).

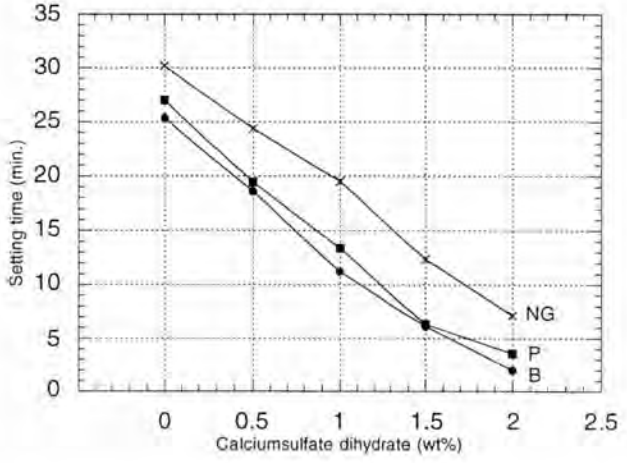

Fig. 4.32 Relationship between initial setting time of MP and the content of calcium sulfate dihydrate (W/P = 0.9).

Table 4.10 Effect of content of potassium sulfate on setting time of MP (humidity = 74%, room and water temperatures = 20°C and 25°C, pH of water = 7.63, W/P = 0.9).

Potassium sulfate (wt%)	Flowability			Setting time (min.)					
				Initial			Final		
	B	P	NG	B	P	NG	B	P	NG
0.00	good	good	good	24.11	25.58	32.26	62.47	78.10	43.20
0.50	good	good	good	19.26	19.21	25.25	48.09	53.45	38.36
1.00	good	good	good	14.35	13.27	19.39	33.14	47.28	23.27
1.50	medium	medium	good	8.15	8.32	12.54	27.36	32.23	15.45
2.00	poor	poor	medium	5.27	5.41	8.45	23.32	27.22	10.19

* the number of test sample was 3 (DIN 1168).

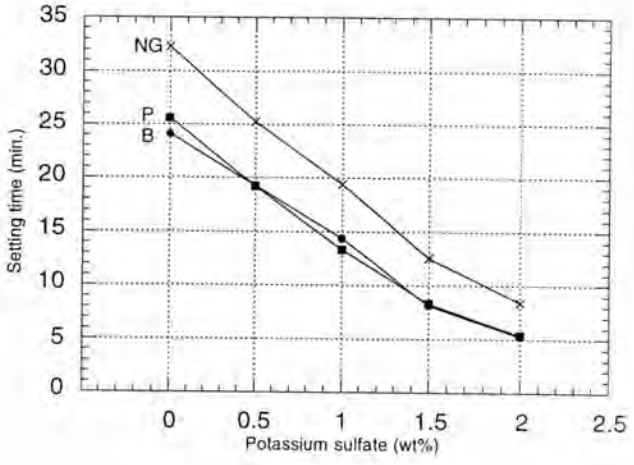

Fig. 4.33 Relationship between initial setting time of MP and the content of potassium sulfate (W/P = 0.9).

Table 4.11 Effect of content of sulfuric acid on setting time of MP (humidity = 67%, room and water temperatures = 19°C and 24°C, pH of water = 7.41, W/P = 0.9).

Sulfuric acid (wt%)	Flowability			Setting time (min.)					
				Initial			Final		
	B	P	NG	B	P	NG	B	P	NG
0.00	good	good	good	26.45	27.18	31.23	68.10	77.42	43.56
0.50	good	good	good	18.16	19.45	24.55	53.45	62.30	33.35
1.00	good	good	good	12.38	13.20	19.27	45.27	57.56	24.20
1.50	medium	medium	good	7.34	7.56	13.40	31.38	41.40	16.47
2.00	poor	poor	medium	3.51	4.11	8.01	26.16	30.27	12.09

* the number of test sample was 3 (DIN 1168).

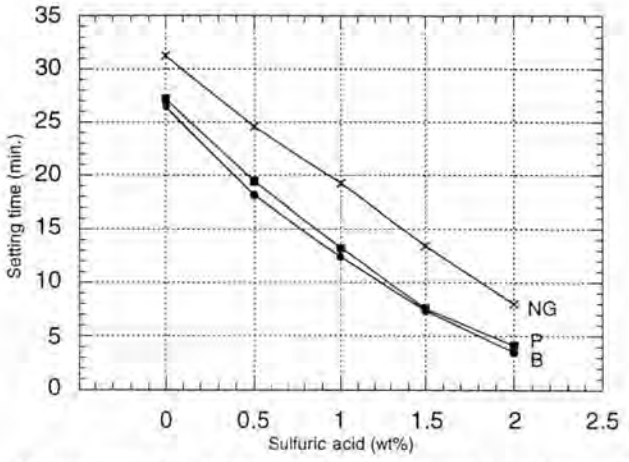

Fig. 4.34 Relationship between initial setting time of MP and the content of sulfuric acid (W/P = 0.9).

Fig. 4.32–4.34 showed that the setting time of MP decreased with increasing content of additives which acted as an accelerator. The initial setting time of MP could be regulated suitably for the application of gypsum board (5–8 min) by adjusting the content of additives. Comparison between the addition of calcium sulfate dihydrate with those of potassium sulfate and sulfuric acid suggested that the first one be a better accelerator since it strongly decreased the initial setting time. The content of additive that regulated the setting of gypsum specimen suitable for the application of gypsum board was shown in Table 4.12.

Table 4.12 Setting time of gypsum board specimens containing the mixture of MP and suitable amount of additives as accelerator (humidity = 74%, room and water temperatures = 20°C and 25°C, pH of water = 7.63, W/P = 0.9).

Additives	Content (wt%)			Setting time (min.)					
				Initial			Final		
	B	P	NG	B	P	NG	B	P	NG
None	-	-	-	27.30±0.26	28.40±0.31	30.40±0.38	65.17±0.36	45.38±0.42	73.26±0.35
Calcium sulfate dihydrate	1.5	1.5	2.0	6.20±0.31	6.42±0.29	7.22±0.22	29.01±0.46	36.47±0.36	12.01±0.42
Potassium sulfate	1.5	1.5	2.0	7.39±0.24	8.03±0.40	8.19±0.31	32.12±0.38	42.50±0.27	12.20±0.36
Sulfuric acid	1.5	1.5	2.0	8.23±0.25	8.36±0.21	8.50±0.45	28.45±0.38	33.45±0.45	10.45±0.39
	2.0	2.0	-	5.35±0.36	5.52±0.32	-	23.45±0.42	27.45±0.39	-

* repeat with 5 tests in each composition.

Hubert (1994) reported that finely ground gypsum dihydrate added to gypsum plasters accelerated the setting process and modified the crystallization of gypsum plasters back into fine crystal of DH, causing the increase in strength. To prove this description, particle morphology and flexural strength of MP added with additives should be investigated.

4.5.2 Particle morphology of DH obtained after the rehydrate of β-HH and MP

a.) Particle morphology of DH after the rehydration of β-HH.

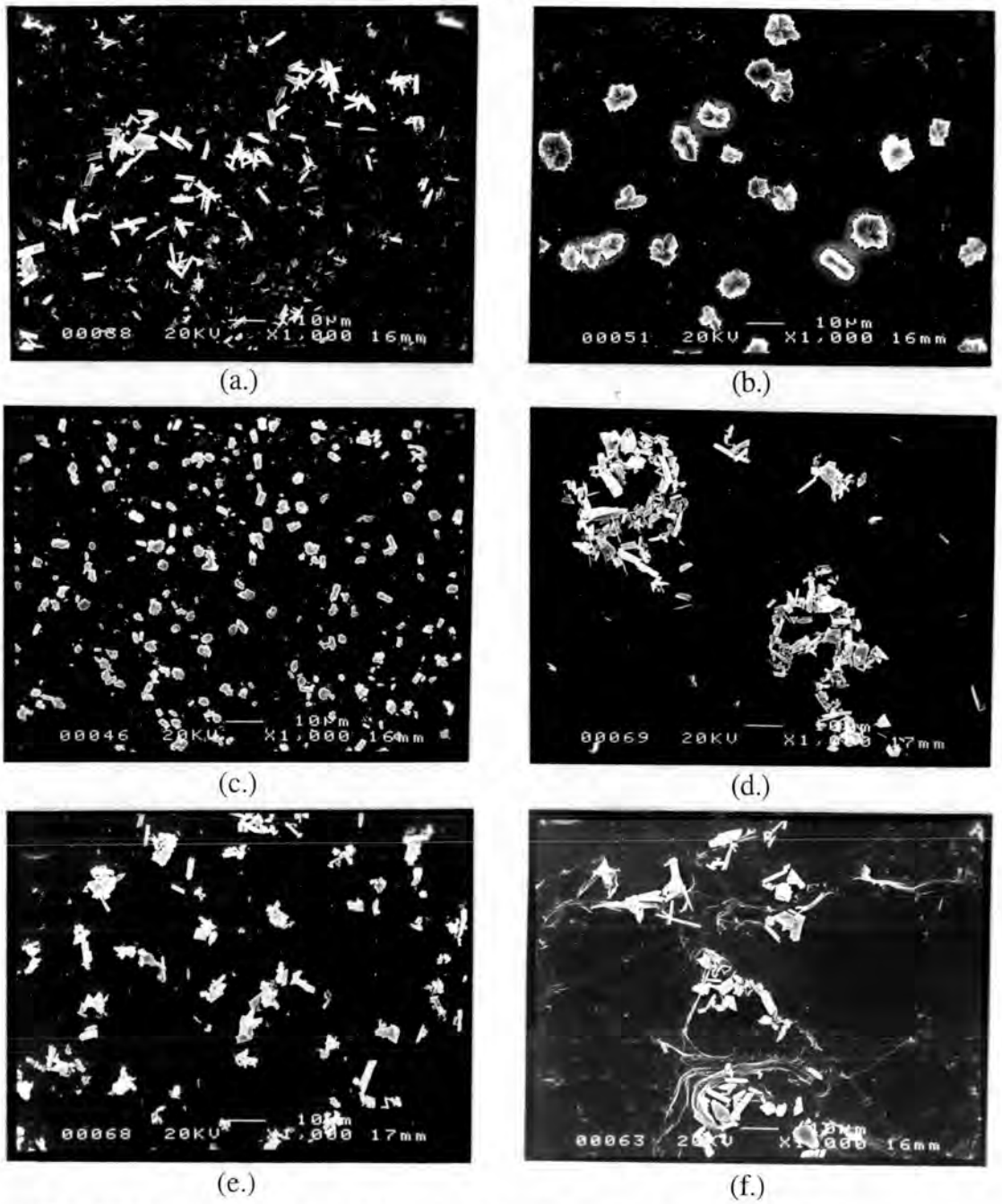

Fig. 4.35 SEM micrographs of hydrated β-HH (FG) with additives a.) no additive, b.) 0.02 wt% citric acid, c.) 0.02 wt% methylcellulose, d.) 0.2 wt% acetic acid, e.) 0.2 wt% potassium alum and f.) 0.2 wt% sodium borate.

(a.)

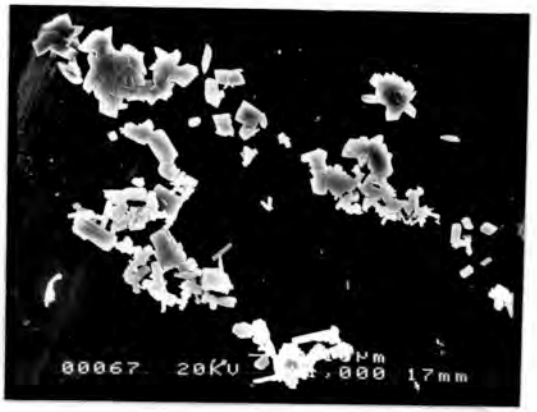

(b.)

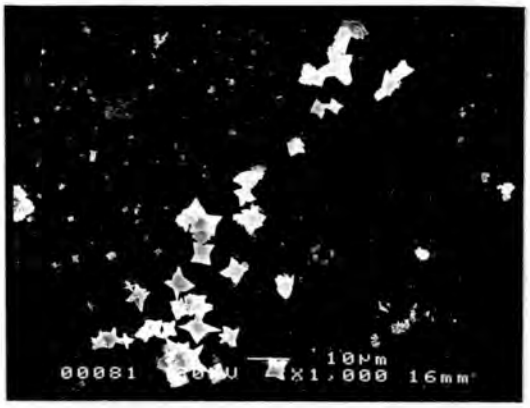

(c.)

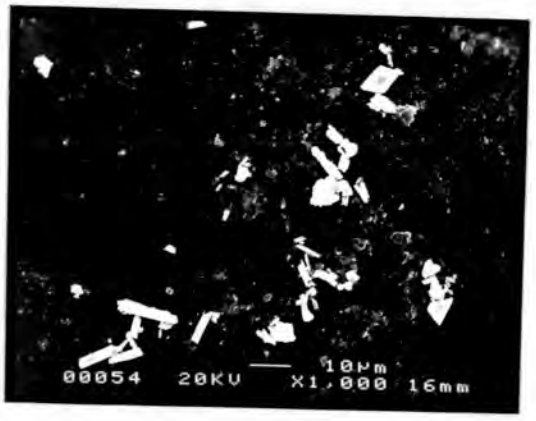

(d.)

(e.)

(f.)

Fig. 4.36 SEM micrographs of hydrated β-HH (NG) with additives a.) no additive, b.) 0.02 wt% citric acid, c.) 0.02 wt% methylcellulose, d.) 0.2 wt% acetic acid, e.) 0.2 wt% potassium alum and f.) 0.2 wt% sodium borate.

Fig. 4.35 and 4.36 showed that with increasing addition of additives, the crystal size of β-HH increased. Especially, addition with citric acid and methylcellulose had changed the morphology from long prismatic to compact-shaped crystals.

b.) Particle morphology of DH after the rehydration of MP

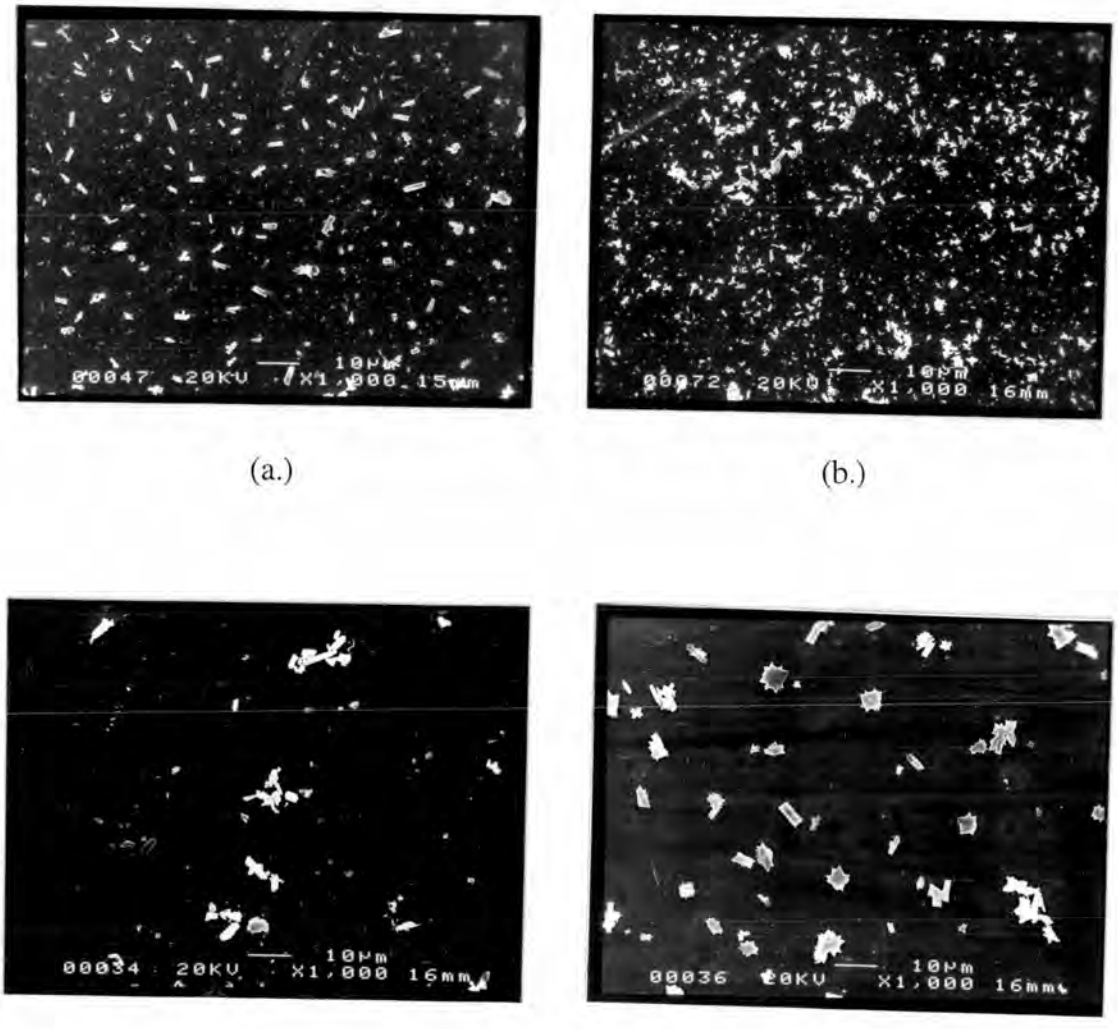

(a.) (b.)

(c.) (d.)

Fig. 4.37 SEM micrographs of hydrated MP (B) with additives
a.) no additive, b.) 1.5 wt% calcium sulfate dihydrate
c.) 1.5 wt% potassium sulfate and d.) 1.5 wt% sulfuric acid.

(a.)

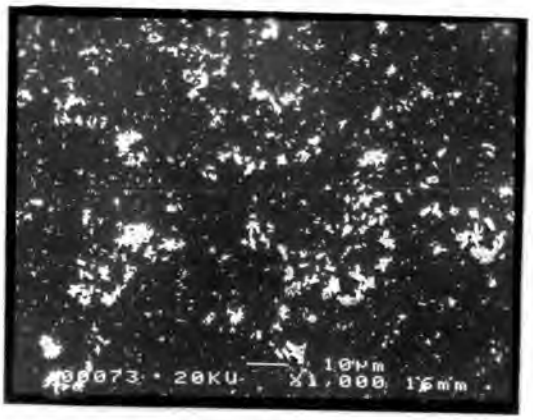

(b.)

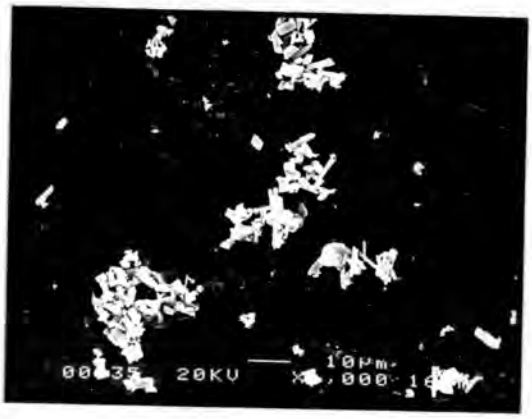

(c.)

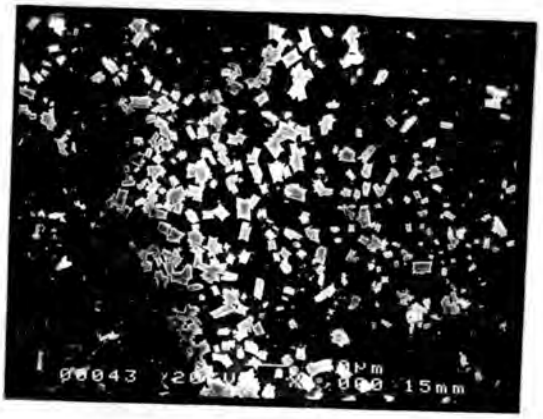

(d.)

Fig. 4.38 SEM micrographs of hydrated MP (P) with additives
a.) no additive, b.) 1.5 wt% calcium sulfate dihydrate
c.) 1.5 wt% potassium sulfate and d.) 1.5 wt% sulfuric acid.

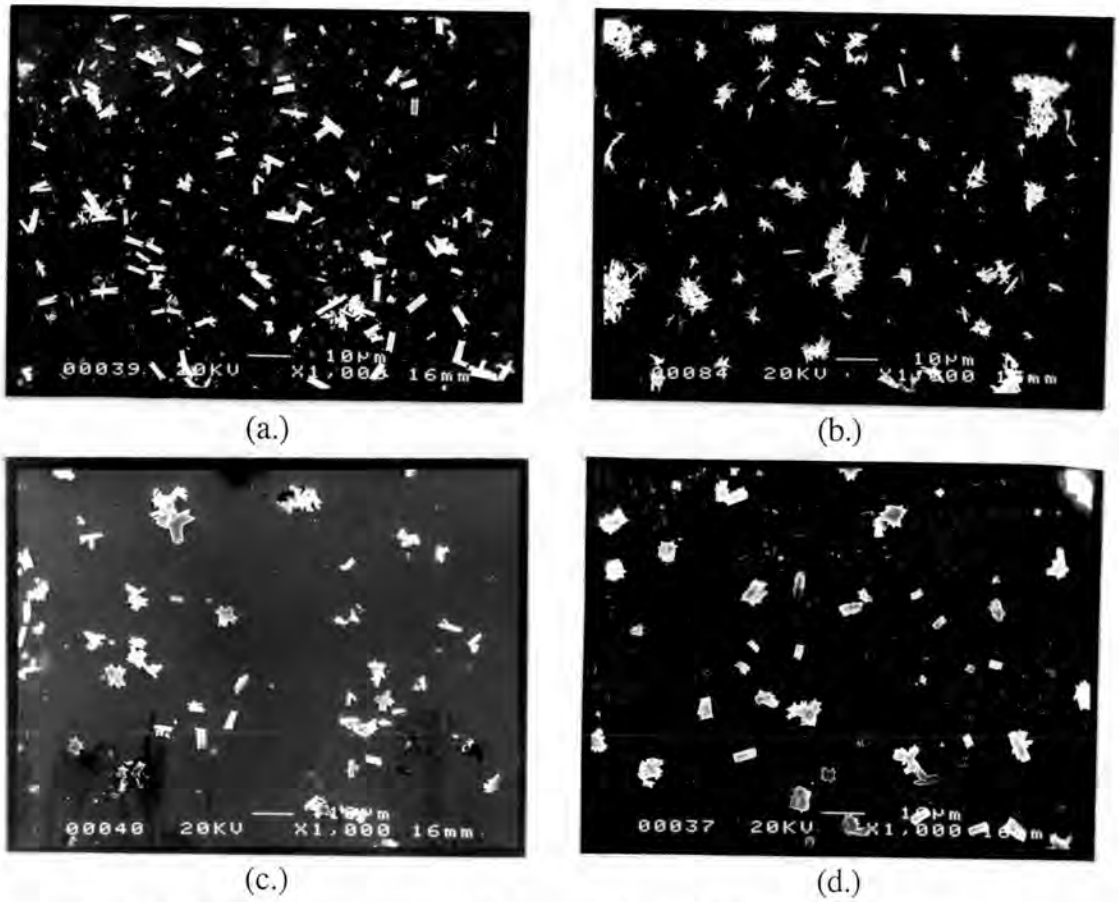

(a.) (b.)

(c.) (d.)

Fig. 4.39 SEM micrographs of hydrated MP (NG) with additives
a.) no additive, b.) 2.0 wt% calcium sulfate dihydrate
c.) 2.0 wt% potassium sulfate and d.) 2.0 wt% sulfuric acid.

Fig. 4.37–4.39 showed that additions with potassium sulfate and sulfuric acid gave large and coarse crystals of DH. But addition with calcium sulfate dihydrate, fine crystals were indicated because it acted as seed, providing a medium for the dissolved gypsum to attach to and grow.

4.5.3 Physical properties of gypsum specimens

a.) Gypsum specimens prepared from β–HH powder

Results of the physical properties of gypsum specimens prepared from β–HH powder were tabulated and illustrated in Appendix : Table 10, page 156 and Fig. 4.40–4.42.

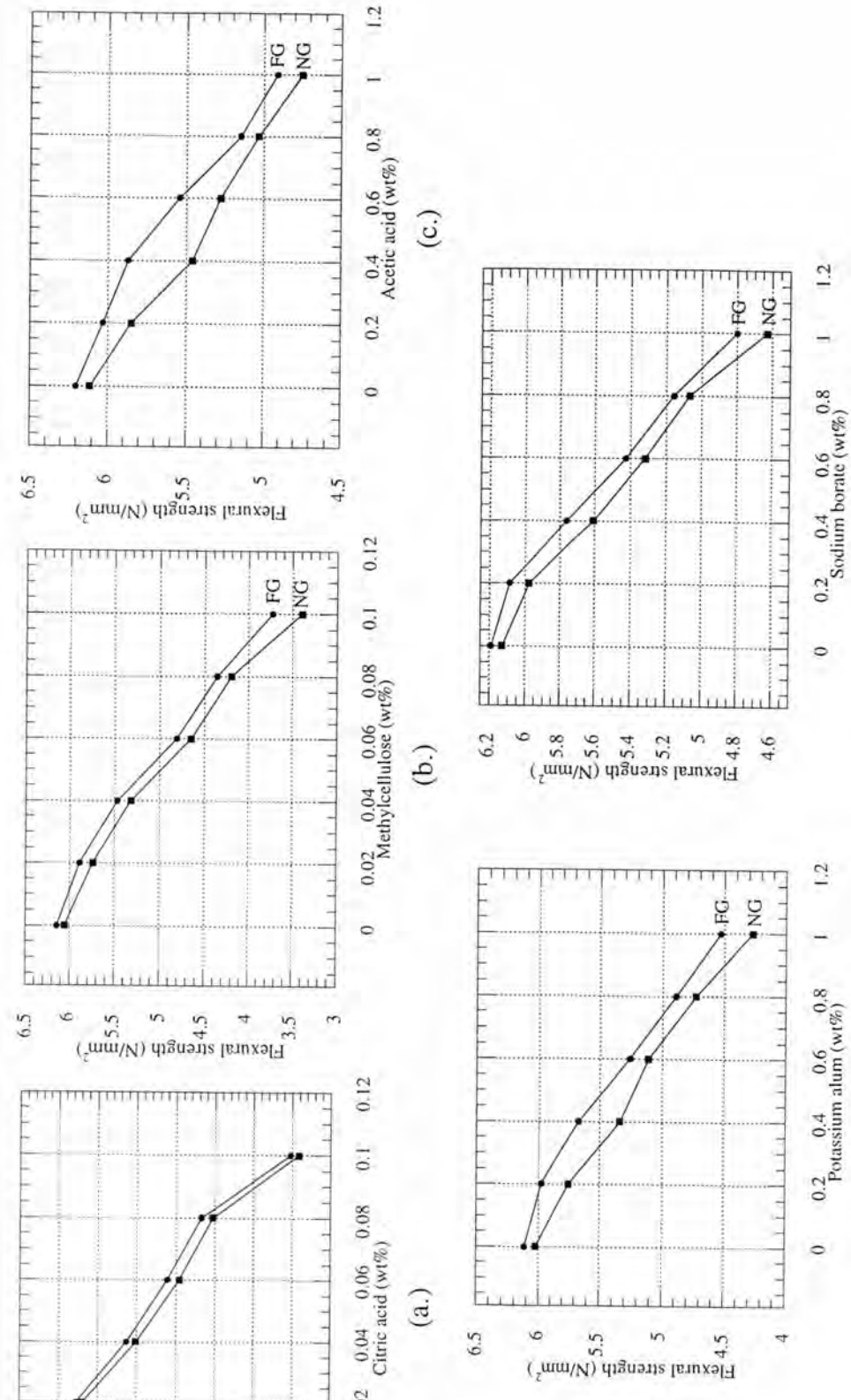

Fig. 4.40 Relationship between the content of additive and the flexural strength of β-HH.
a.) citric acid, b.) methylcellulose, c.) acetic acid, d.) potassium alum and e.) sodium borate.

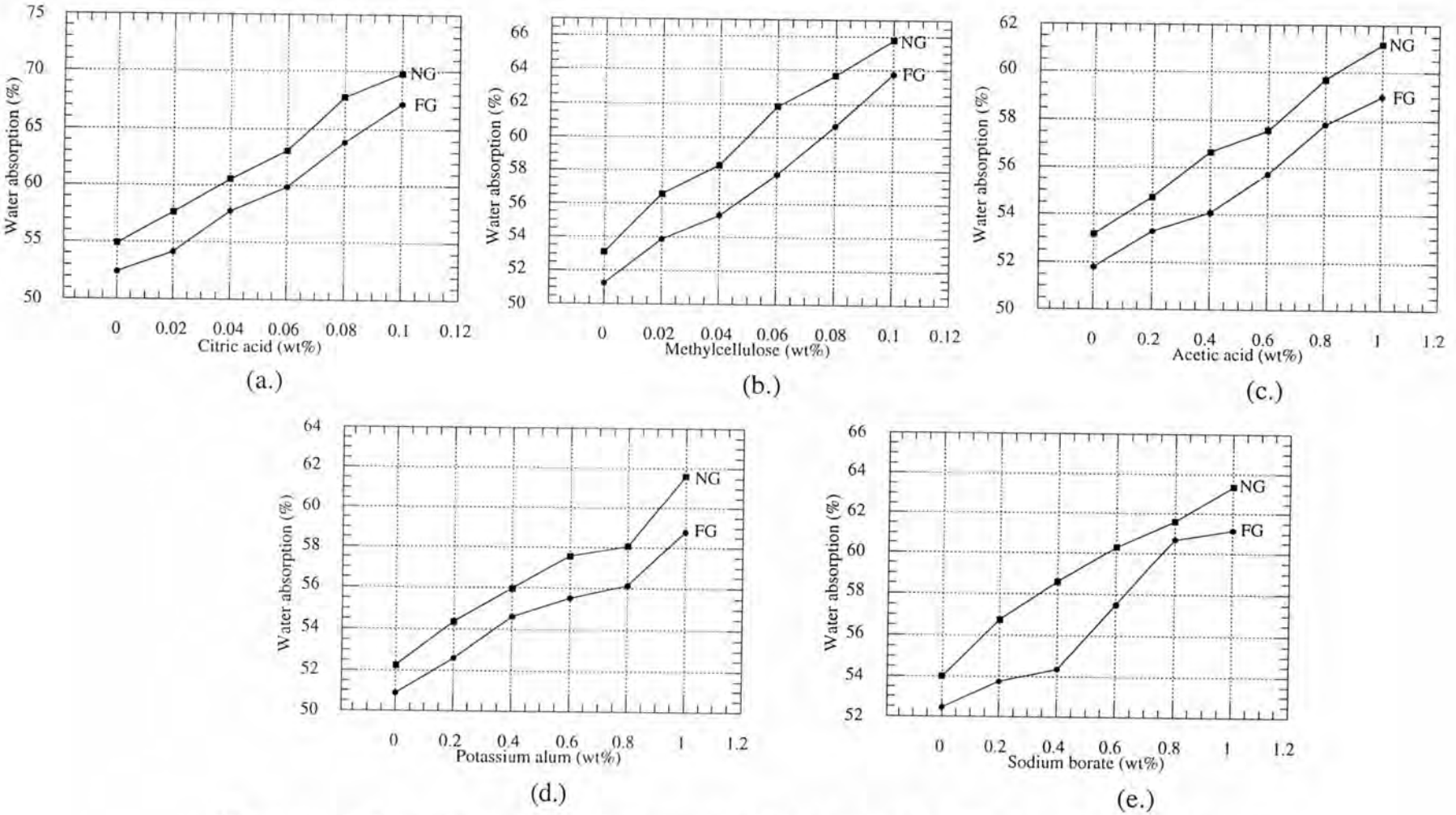

Fig. 4.41 Relationship between the content of additive and the water absorption of β-HH. a.) citric acid, b.) methylcellulose, c.) acetic acid, d.) potassium alum and e.) sodium borate.

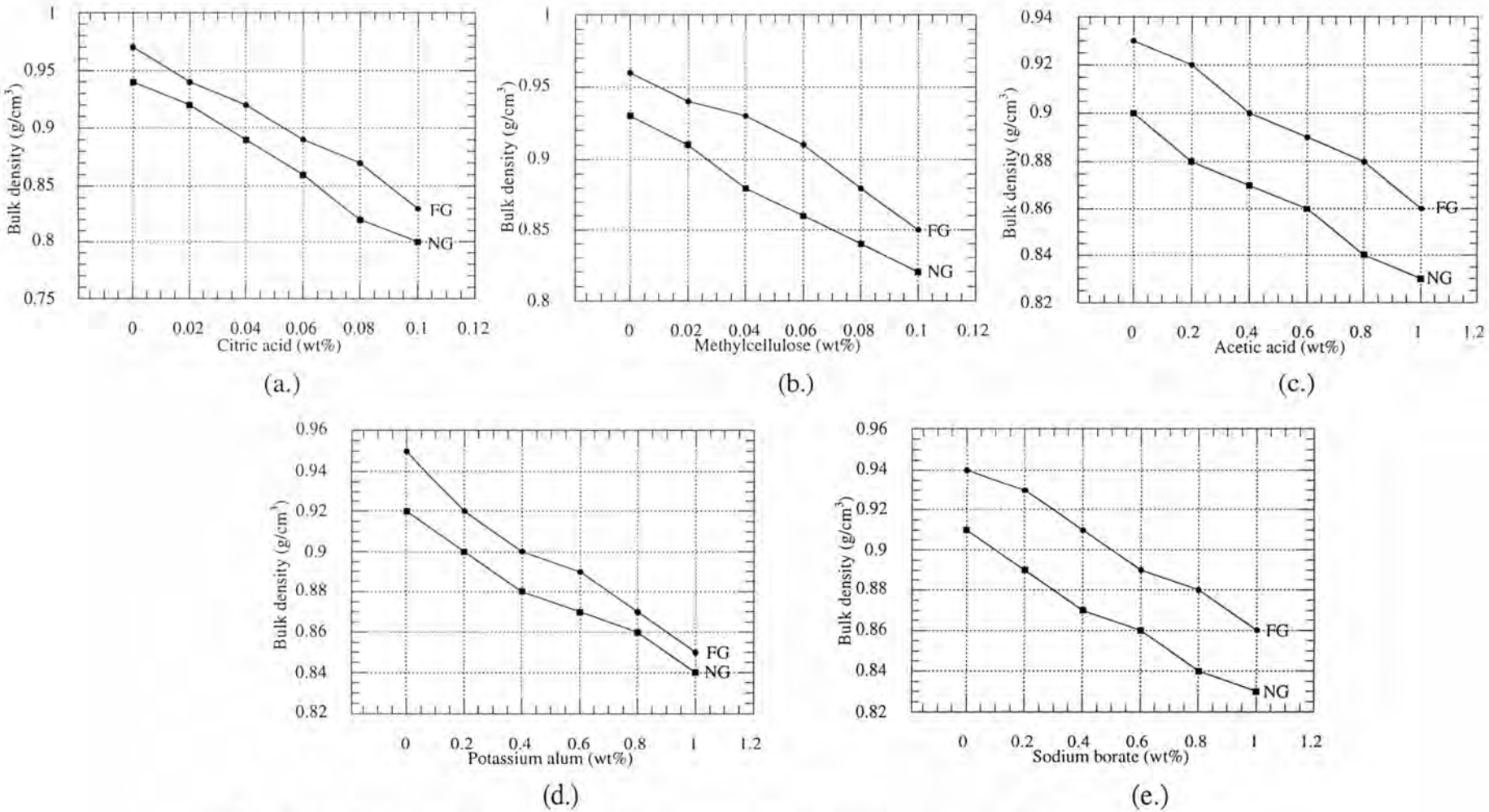

Fig. 4.42 Relationship between the content of additive and the bulk density of β-HH.
a.) citric acid, b.) methylcellulose, c.) acetic acid, d.) potassium alum and e.) sodium borate.

Fig. 4.40 was the plots between the content of additive (wt%) and the flexural strength (N/mm^2). It was found from the plots that the flexural strength decreased with increase of additive content, especially, addition with citric acid and methylcellulose. The flexural strength was strongly reduced due to morphology and size of the hydrate crystal which were indicated in Fig. 4.35 and 4.36. This was also confirmed by the results of water absorption and bulk density (Fig. 4.41 and 4.42). It was found that the increase of additive content increased the water absorption and hence reduced the bulk density.

Kuhlmann and Ludwig (1977) supported these results, They reported that the addition of some retarding or accelerating agents did not only cause the change in structure but also increased the average pore size and air bubble diameter in gypsum products.

b.) Gypsum board specimens prepared from MP

Results of the physical properties of gypsum board specimens prepared from MP were tabulated and illustrated in Appendix : Table 11, page 157 and Fig. 4.43-4.45.

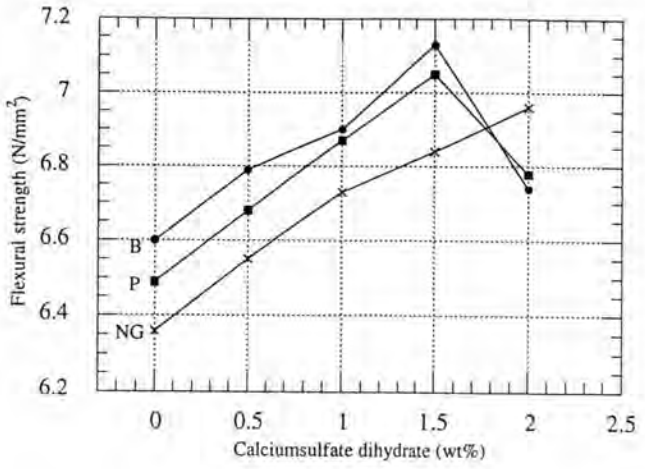

(a.)

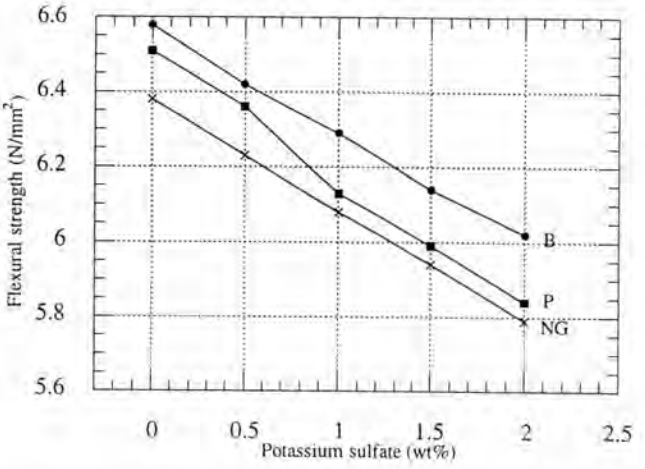

(b.)

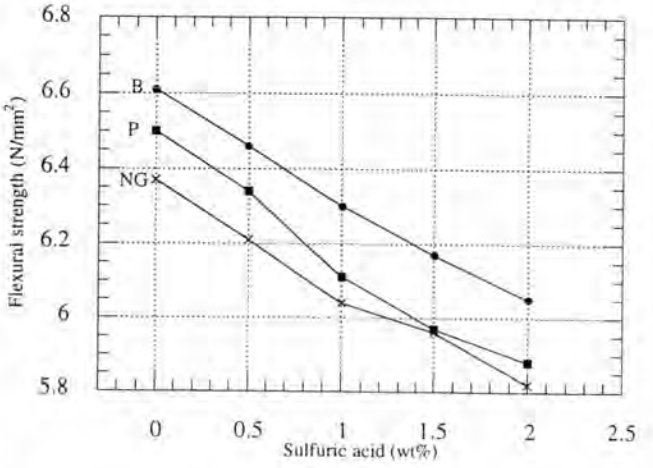

(c.)

Fig. 4.43 Relationship between the flexural strength of MP and content of additive a.) calcium sulfate dihydrate, b.) potassium sulfate and c.) sulfuric acid.

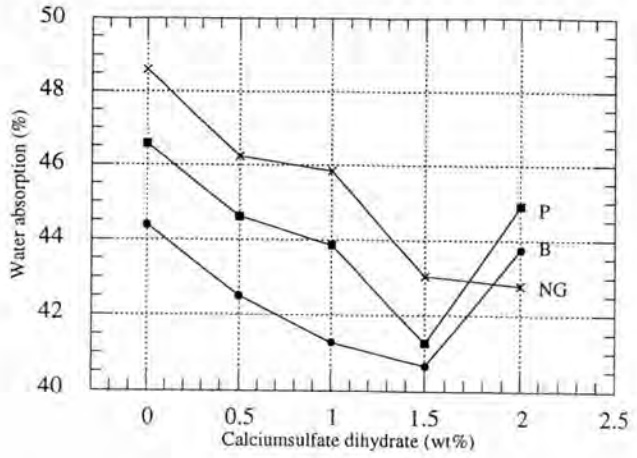

(a.)

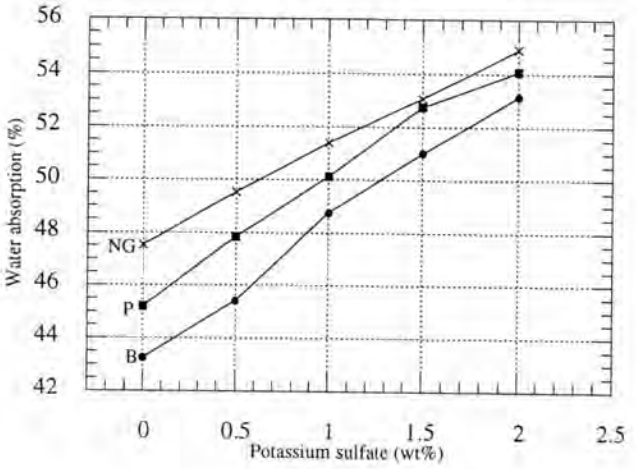

(b.)

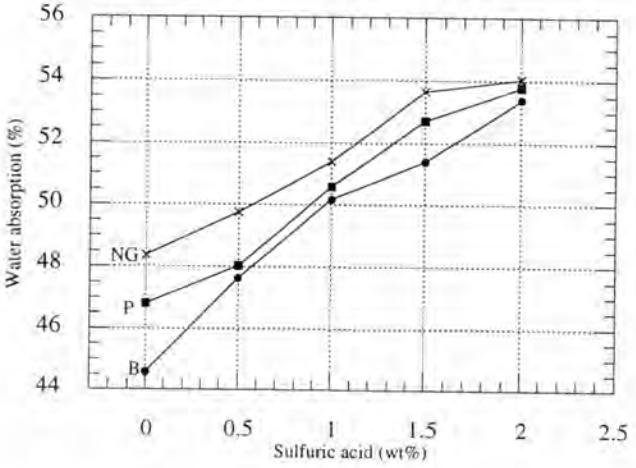

(c.)

Fig. 4.44 Relationship between the water absorption of MP and the content of additive a.) calcium sulfate dihydrate, b.) potassium sulfate and c.) sulfuric acid.

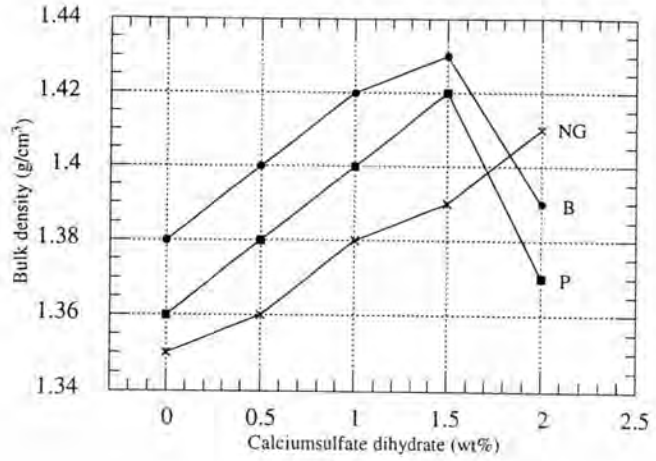

(a.)

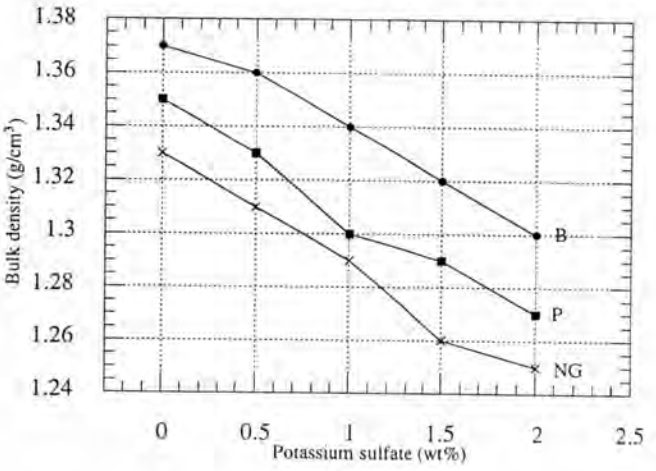

(b.)

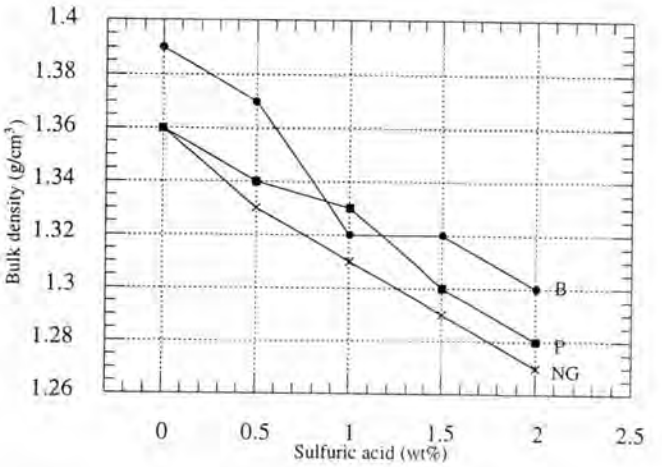

(c.)

Fig. 4.45 Relationship between bulk density of MP and the content of addive a.) calcium sulfate dihydrate, b.) potassium sulfate and c.) sulfuric acid.

Fig. 4.43 showed the effect of the content of additive on the flexural strength of gypsum specimens. It was found that the flexural strength decreased with increase of the contents of potassium sulfate and sulfuric acid but the addition of calcium sulfate dihydrate increased the flexural strength and the maximum strength was obtained at 1.5, 1.5 and 2.0 wt% of calcium sulfate dihydrate for B, P and NG, respectively, probably due to the formation of fine crystals of gypsum (Fig. 4.37-4.39). These results were also confirmed by the results of the water absorption and the bulk density (Fig. 4.44 and 4.45).

The drop of flexural strength with higher contents of calcium sulfate dihydrate was explained by Jinawath et al. (1996) that too high content of dihydrate severely shortened the initial setting time and hence permitted not enough time to prepare a complete test specimen. The other reason was described by Hubert (1994) that the excess amount of calcium sulfate dihydrate did not introduce the fine crystals of gypsum and this would affect the strength.

4.5.4 Effect of humidity on the flexural strength of gypsum board specimen

Table 4.13 showed the effect of humidity on the flexural strength of gypsum board specimens which were exposed to 98% humidity for 49 days. It was found that the flexural strength of gypsum board specimens decreased. this result was described by Albrecht (1953) that the strength of gypsum products with a moisture content exceeding 5% was only about one half that of air-dried gypsum products. This was explained by Wandser (1962) that the moist conditions reduced strength because of the crystalline and textural changes, especially recrystallization taking place as a result of the solubility of gypsum in water. The deformation or creep of moist gypsum products under mechanical stress was likewise the result of

structural change. However, The drop of strength of specimens with 1.5-2.0 wt% additive was far less than 50% of the original value.

Table 4.13 Effect of humidity on the flexural strength of gypsum specimen (exposed to 98% humidity for 49 days).

Gypsum specimen	Calcium sulfate dihydrate (wt%)	Flexural strength (N/mm^2)		Moisture content in specimens (%)	Flexural strength reduced (%)
		Dried gypsum specimens	exposed to 98% humidity for 49 days		
B	-	6.60	3.85	7.98	41.67
	1.5	7.13	5.42	9.31	23.98
P	-	6.49	3.60	7.96	44.53
	1.5	7.05	5.23	8.25	24.26
NG	-	6.36	3.41	8.73	46.38
	2.0	6.84	4.98	10.30	27.19

4.6 Preparation of projection plaster from MP

4.61 Preparation of MP for projection plaster

a.) Effect of grinding time on the particle size of MP

Results of the grinding time on the particle size of MP were shown in Appendix : Table 12, page 158 and Fig. 4.46.

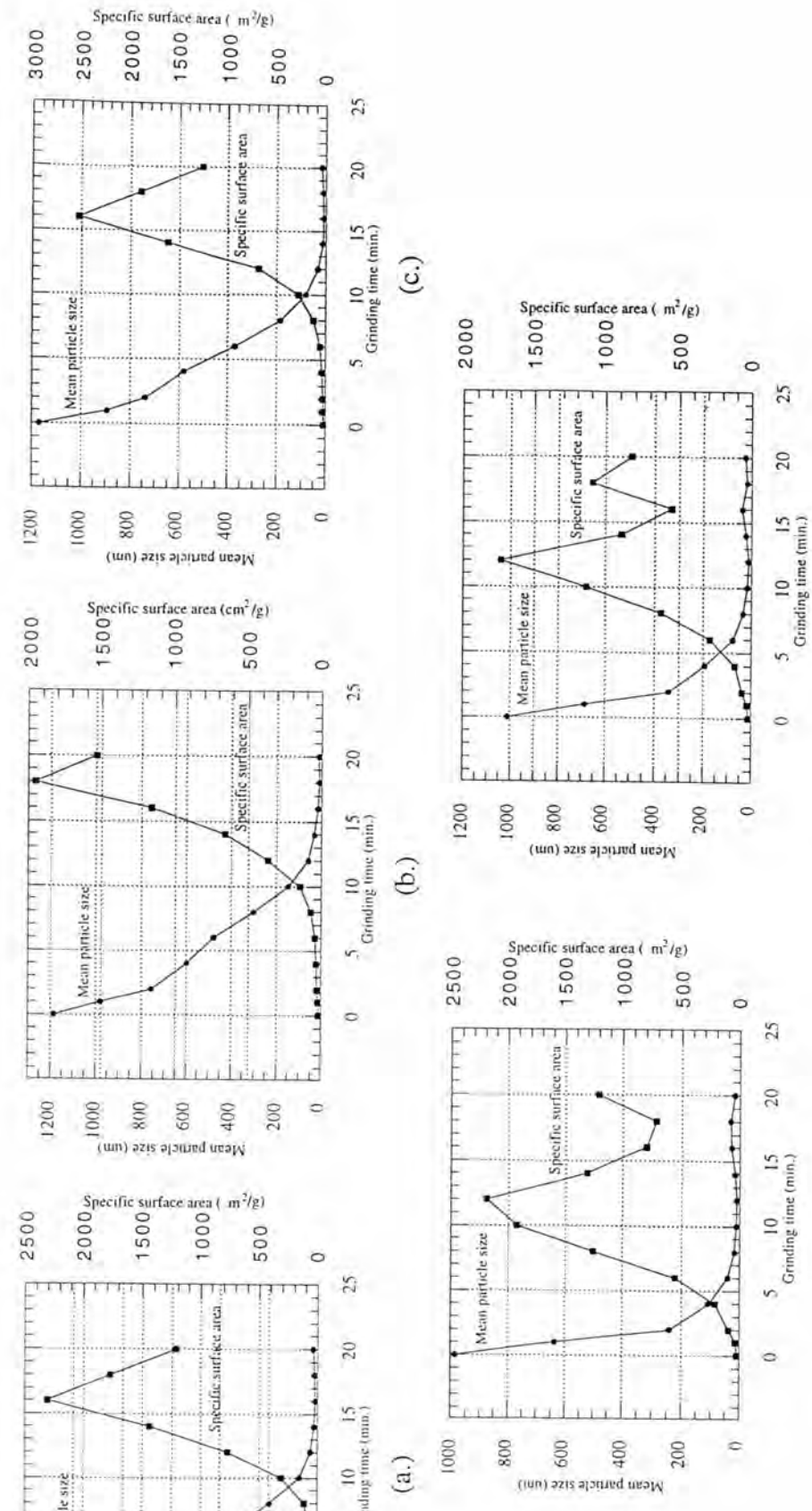

Fig. 4.46 Effect of grinding time on the specific surface area and mean particle size of MP prepared from a.) B, b.) P, c.) NG, d.) mixed phase of FG and e.) mixed phase of NG.

Fig. 4.46 showed the particle size of MP obtained from the calculation based on specific surface area after grinding at various times. It was found that the particle size of MP was reduced with increasing grinding time but grinding with prolonged time could cause increase in particle size because of the reagglomeration of particles. Love (1972) reported that materials suitable for projection plaster were fine powder of which all particles were below 20 μm in size.

Following his report, the minimum time that gave the particle size of MP below 20 μm was chosen from the results in Appendix : Table 12. An example of ground powder at the chosen grinding time was analysed by centrifugal particle size analyzer to confirm the results of Appendix : Table 12. The results were shown in Appendix : Table 13, page 159 and Fig. 4.47.

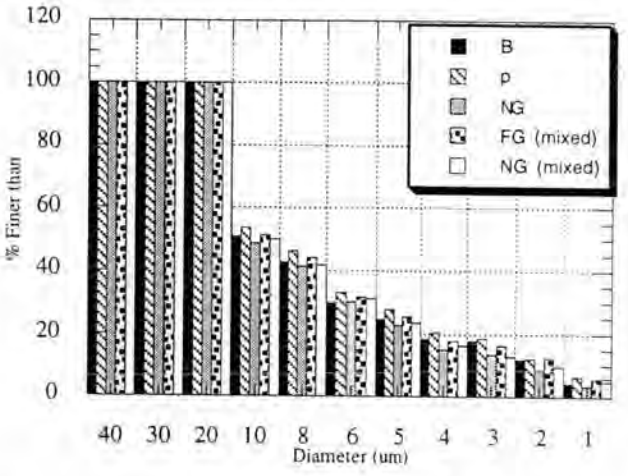

Fig. 4.47 Particle size distribution of MP from centrifugal particle size analyzer, presented as histogram.

b.) Preparation of gypsum specimens from MP (DIN 1164)

Results of the setting time and physical properties of MP powder were shown in Table 4.14, Appendix : Table 14, page 159 and Fig. 4.48-4.49.

Table 4.14 Effect of the content of methylcellulose on the setting time of MP (humidity = 65%, room and water temperatures = 22°C and 26°C, pH of water = 7.63 and W/P = 0.6).

Methyl cellulose (wt%)	Setting time (min.)									
	Initial					Final				
	B	P	NG	FG (mixed)	NG (mixed)	B	P	NG	FG (mixed)	NG (mixed)
0.00	15.31	17.34	19.53	9.53	14.37	60.58	74.18	29.32	46.09	22.56
0.02	31.26	34.17	37.54	20.08	28.35	100.33	112.43	64.49	77.63	51.40
0.04	50.59	52.35	58.32	38.22	49.42	137.50	149.27	103.28	95.13	86.33
0.06	64.03	68.28	76.39	51.40	60.20	171.37	174.18	122.40	134.27	105.09
0.08	73.48	79.40	91.04	67.28	71.15	183.58	190.34	148.53	172.10	134.46
0.10	90.35	96.36	110.18	84.35	92.38	192.05	201.10	170.11	188.35	170.58

* the number of test sample was 3 (DIN 1168).

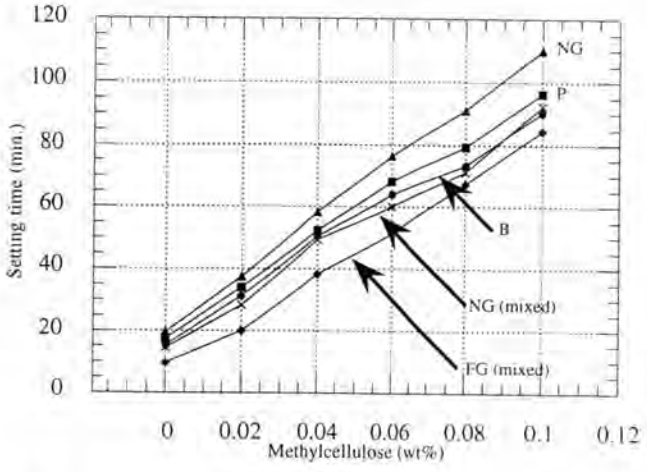

Fig. 4.48 Relationship between the content of methylcellulose and initial setting time of MP prepared from bulk materials and mixed phase composition.

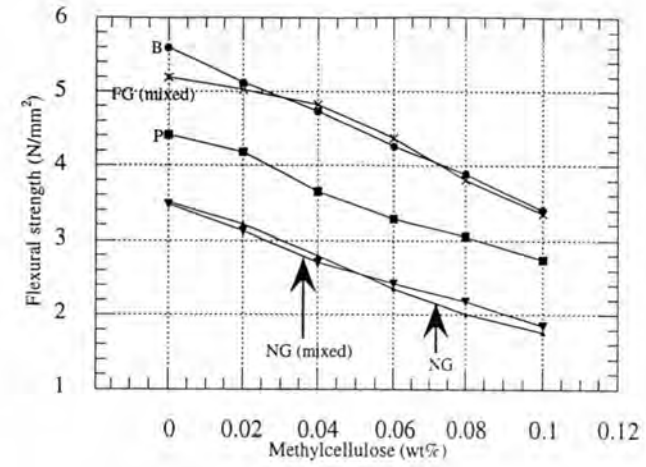

(a.)

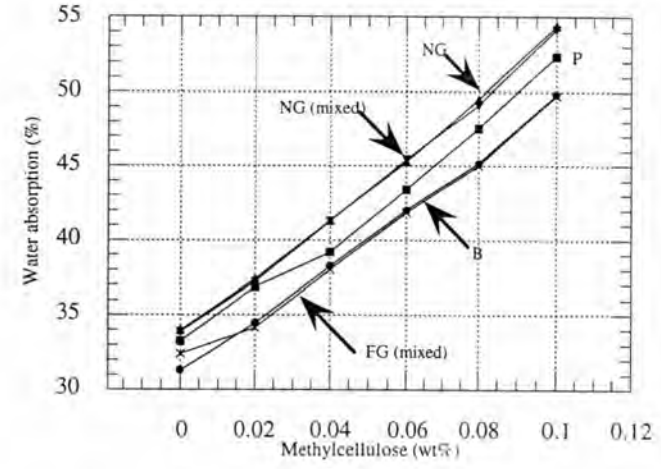

(b.)

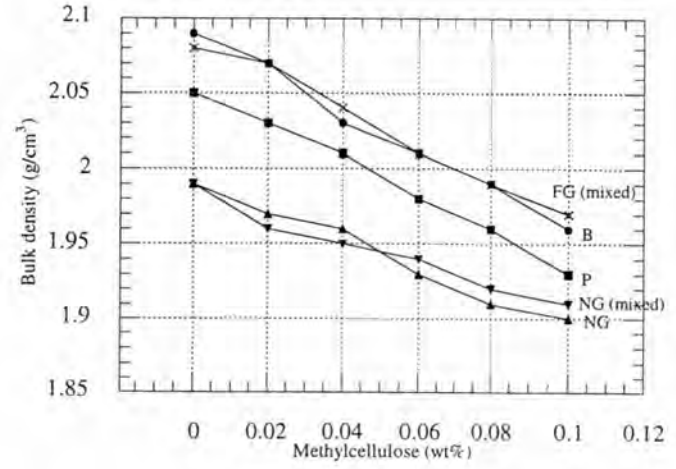

(c.)

Fig. 4.49 Relationship between the content of Methylcellulose and physical properties of MP a.) flexural strength, b.) water absorption and c.) bulk density.

Fig. 4.48 and 4.49 showed the proximate results of setting time and physical properties of both MP which obtained from calcining bulk materials and mixed phase composition. Since β-HH, AIII and AII could not produce as single phase, practically it was not possible to get exact phase composition of MP by mixing them. So, MP which obtained from calcining bulk materials was chosen for the starting material of projection plaster, considering from the uniformity of phase composition.

4.6.2 Typical properties of projection plaster

a.) Viscosity and setting time

The effects of additives on the viscosity and setting time were tabulated and illustrated in Appendix : Table 15, page 160, Fig. 4.50 and 4.52.

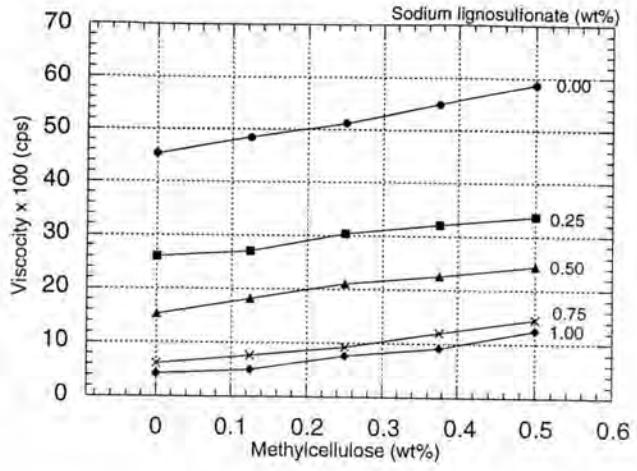

(a.)

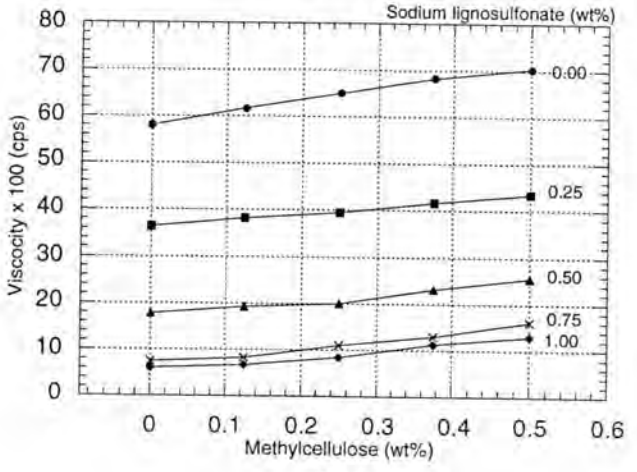

(b.)

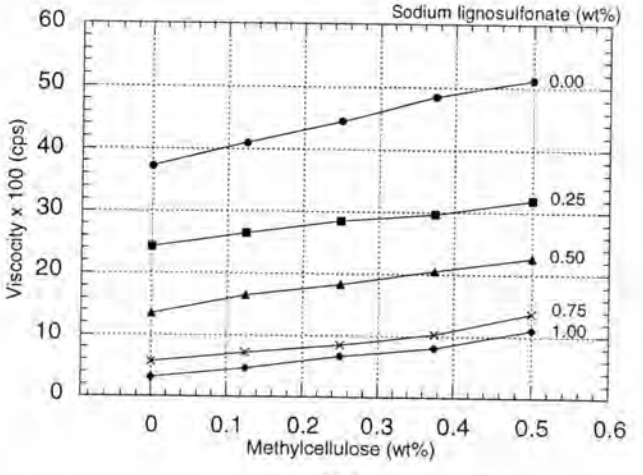

(c.)

Fig. 4.50 Relationship between the content of sodium lignosulfonate + methylcellulose and viscosity of projection plaster which prepared from a.) B, b.) P and c.) NG.

Fig. 4.50 showed that the viscosity of the projection plaster strongly decreased with the content of sodium lignosulfonate but gradually increased with the content of methylcellulose. The viscosity which is suitable for applying the projection plaster was in the range of 600–800 cps. Rixom and Maivaganam (1986) reported that sodium lignosulfonate acted as the water-reducing agent and affected the rheology of gypsum cement paste, it could be seen from Fig. 4.51 that the addition of sodium lignosulfonate did not appeare to alter the shape of the shear stress-shear rate relationship but merely moved it to a lower level. Methylcellulose acted as binder and prevented rapid loss of water into the substrate and into air.

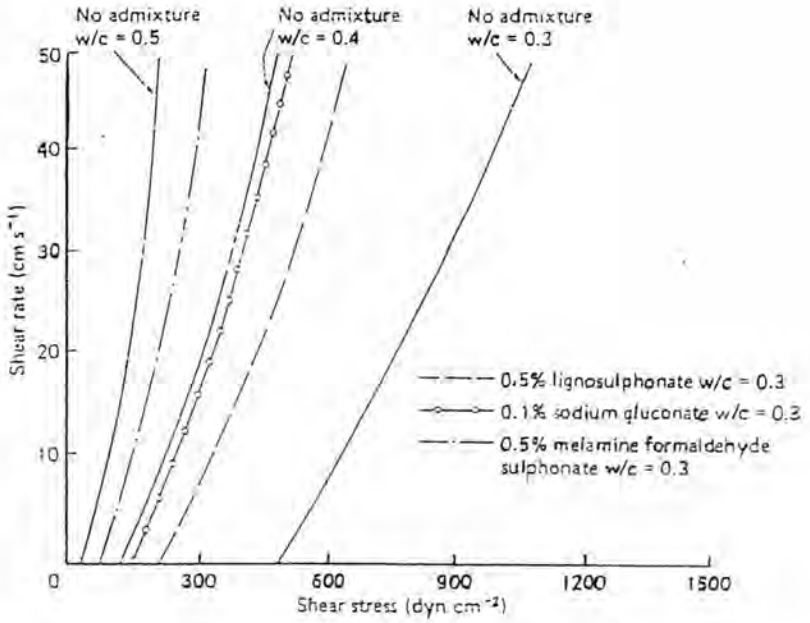

Fig. 4.51 Shear stress and shear rate relationships for gypsum-cement pastes containing water reducing agent.

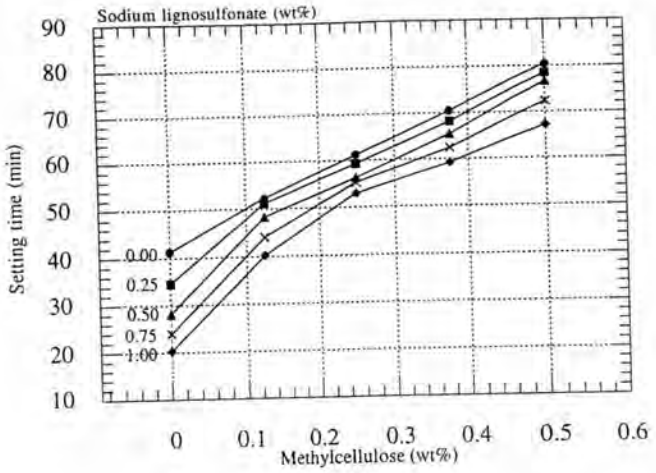

(a.)

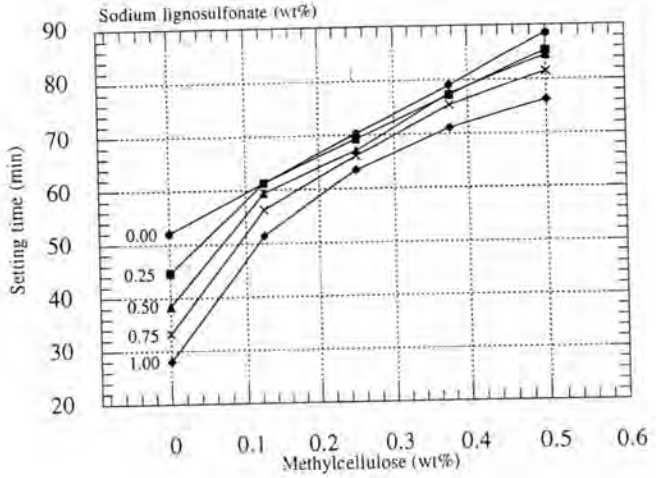

(b.)

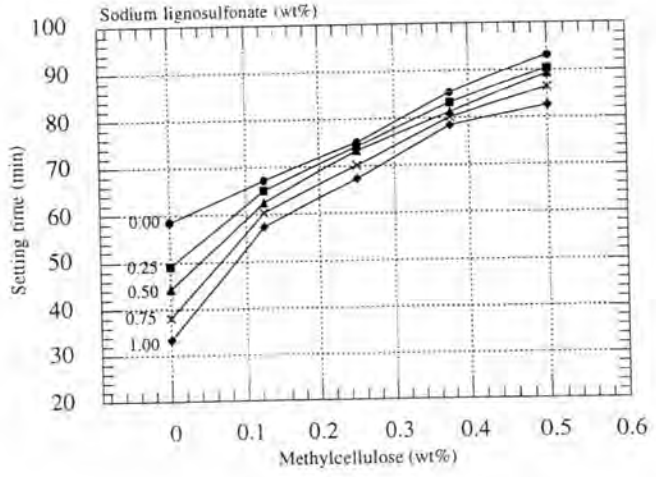

(c.)

Fig. 4.52 Relationship between the content of sodium lignosulfonate + methylcellulose and initial setting time of projection plaster prepared from a.) B, b.) P and c.) NG.

Fig. 4.52 showed that the setting time decreased with the content of sodium lignosulfonate but increased with the content of methylcellulose. The lignosulfonate molecules had retarding influence but the admixture with sodium salt caused accelerating influence. Methylcellulose also had water retention properties, retarding influence to provide long working and application time.

The setting time of projection plaster, Table 2.11, was not in the range that conformed to DIN 1168 (60–120 min for initial setting and 170–220 min for final setting). These might be caused by the effects of ambient and water temperatures which were higher than the test condition specified by DIN and the increase in ambient and water temperature would bring about the increase in the solubility of gypsum plaster (Fig. 2.13).

b.) Surface coverage and surface hardness

The effects of viscosity and the content of additves on surface coverage and surface hardness of projection plaster were indicated in Appendix : Table 16, page 161 and Fig. 4.53.

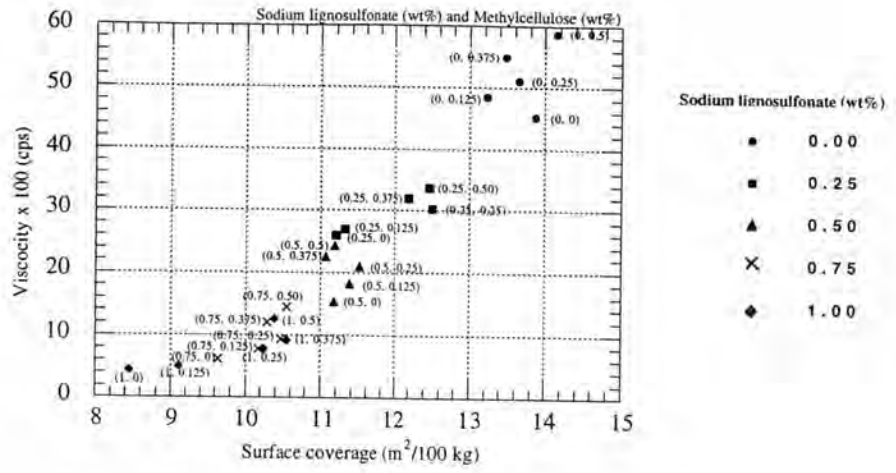

(a.)

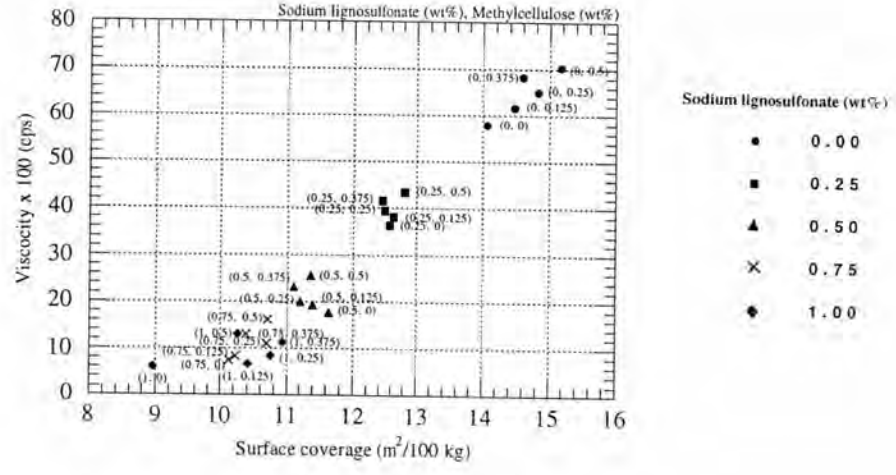

(b.)

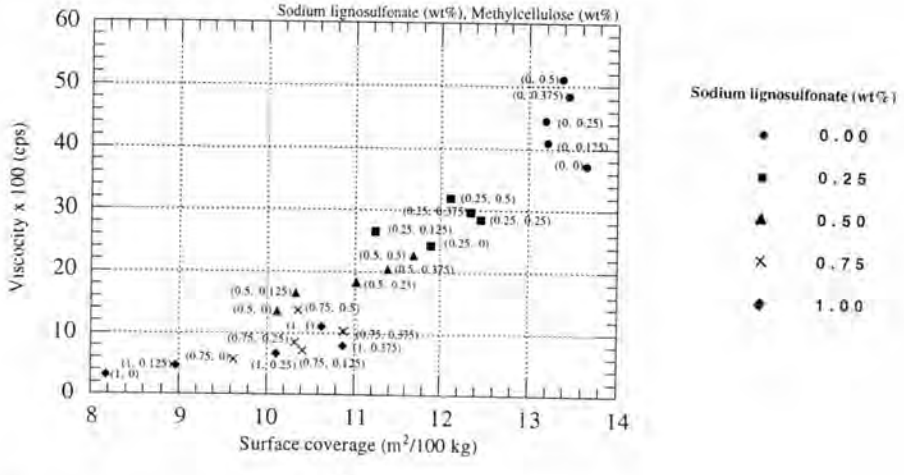

(c.)

Fig. 4.53 Relationship between viscosity and surface coverage of projection plaster prepared from a.) B, b.) P and c.) NG.

Fig. 4.53 indicated that the surface coverage of projection plaster increased with the viscosity and the results covered the range of 9-10 m^2/100 kg, conforming to the DIN 1168. (Table 2.10). Exceptionally, for the addition of 1.00 wt% of sodium lignosulfonate was lower because of too low viscosity and it was not suitable to be applied as projection plaster. The surface hardness of projection plaster was tabulated in Table 4.31. It was found that surface hardness increased with the content of methylcellulose but still the surface hardness of projection plaster was unsatisfactory because it peeled easily. To improve this weakness, additions with both sodium lignosulfonate and methylcellulose in the following ratios : 0.75 : 0.00, 0.75 : 0.125 and 1.00 : 0.25 were experimented to modify the property of projection plaster, these compositions were considered from their viscosity, surface coverage and workability.

c.) Physical properties

Results of the physical properties of projection plaster were tabulated and illustrated in Appendix : Table 17, page 162 and Fig. 4.54-4.56.

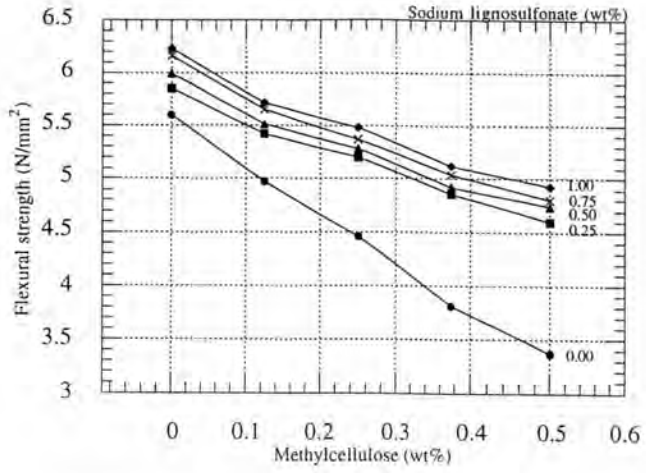

(a.)

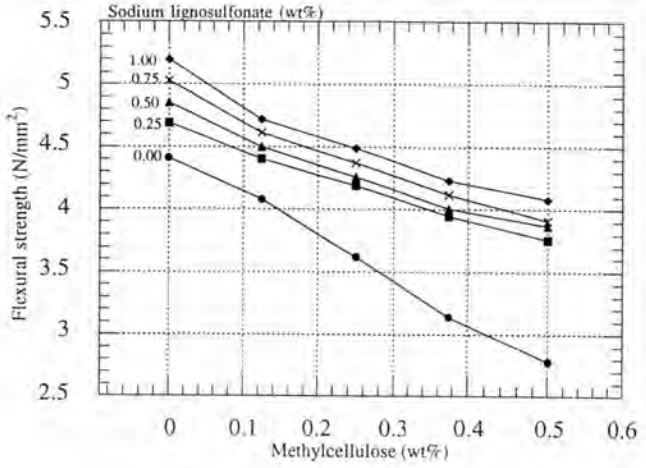

(b.)

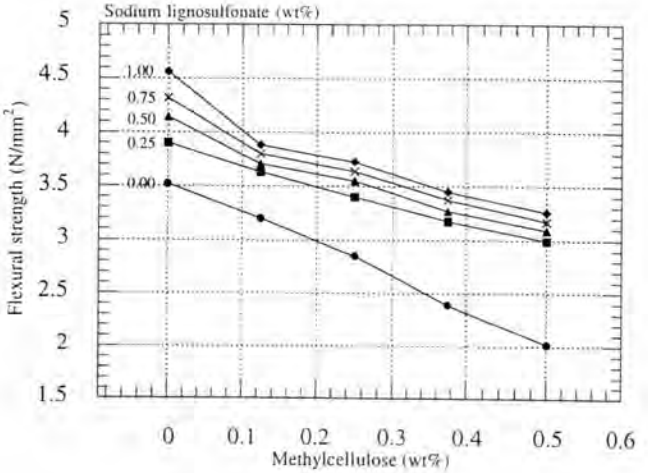

(c.)

Fig. 4.54 Relationship between the content of sodium lignosulfonate + methylcellulose and flexural strength of projection plaster prepared from a.) B, b.) P and c.) NG.

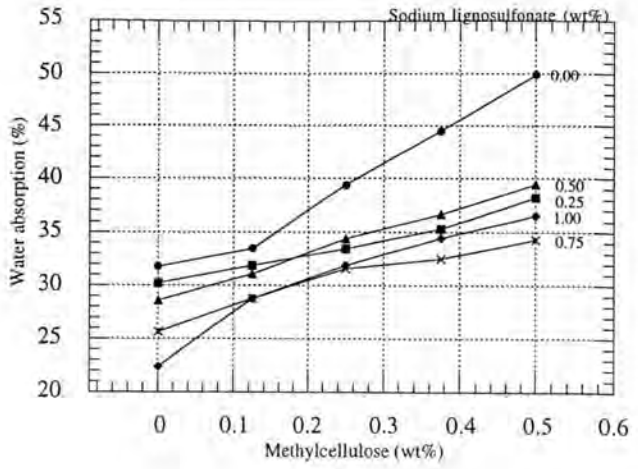

(a.)

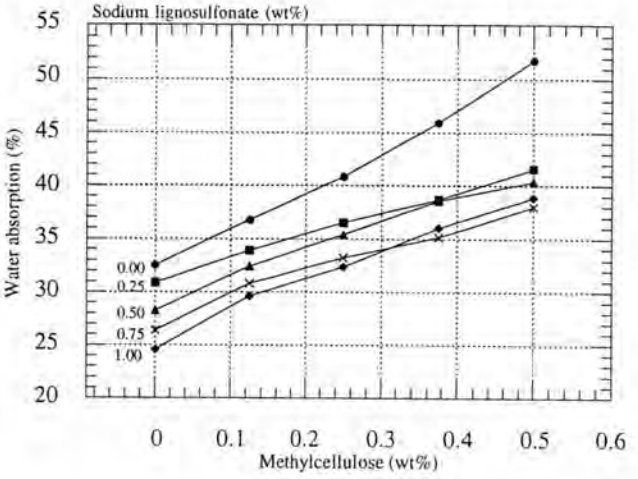

(b.)

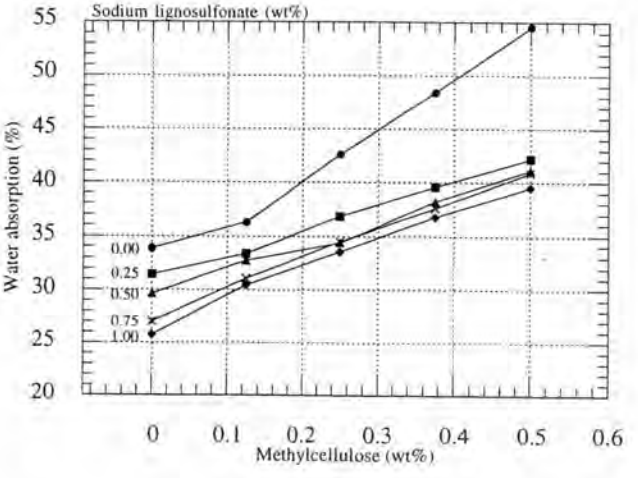

(c.)

Fig. 4.55 Relationship between the content of sodium lignosulfonate + methylcellulose and water absorption of projection plaster prepared from a.) B, b.) P and c.) NG.

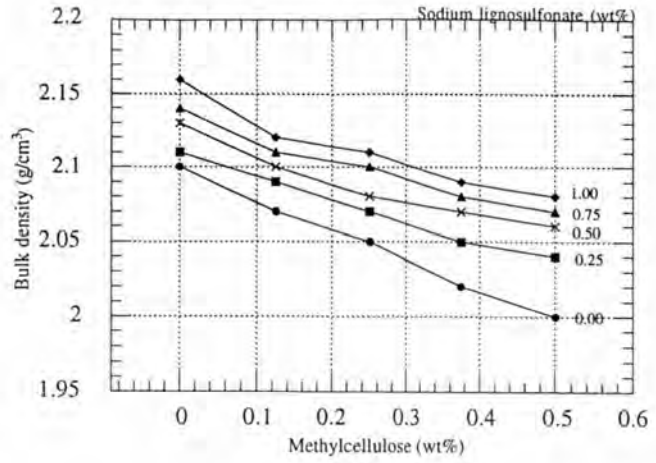

(a.)

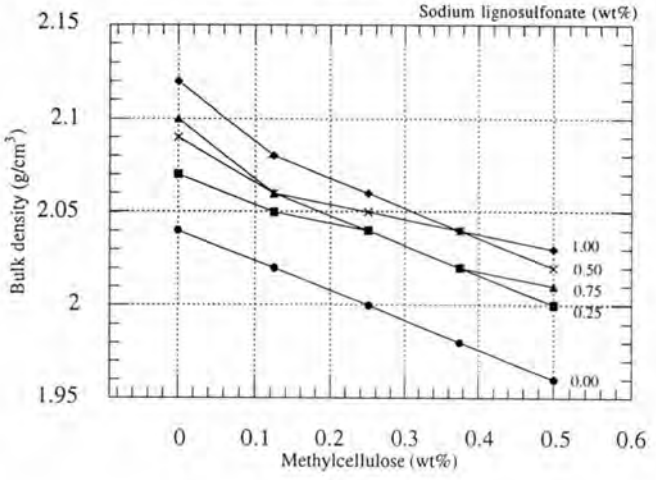

(b.)

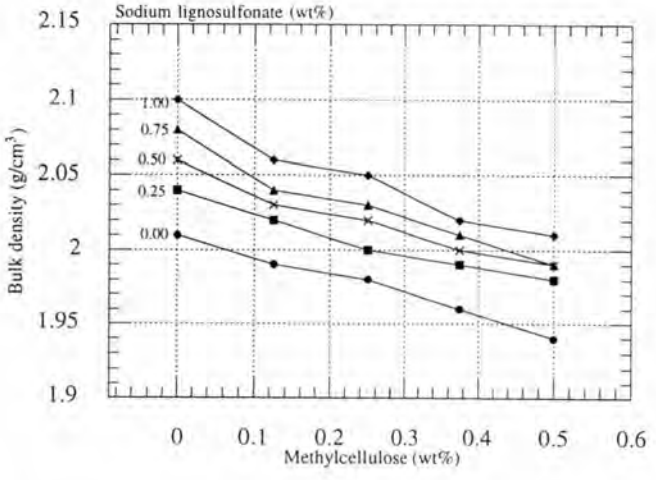

(c.)

Fig. 4.56 Relationship between the content of sodium lignosulfonate + methylcellulose and bulk density of projection plaster prepared rom a.) B, b.) P and c.) NG.

Fig. 4.54 showed that the flexural strength sligthly increased with the content of sodium lignosulfonate but decreased with the increase of of methylcellulose. This might be caused by sodium lignosulfonate also acted as dispersing agent, leading to well distribution of MP particles to react with water increasing the rehydration rate. On the other hand, methylcellulose was absorbed onto the MP particles and prevented them to react with water, leading to low rehydration.

These results were confirmed by the results of water absorption and bulk density (Fig. 4.55 and 4.56). It was found that when the flexural strength increased, the water absorption decreased and hence the bulk density increased.

4.6.2 Modification of projection plaster

a.) Viscosity and setting time

Results of modification of projection plaster by addition of vinyl acetate which affected the viscosity and setting time were shown in Appendix : Table 18, page 163 and Fig. 4.57-4.58.

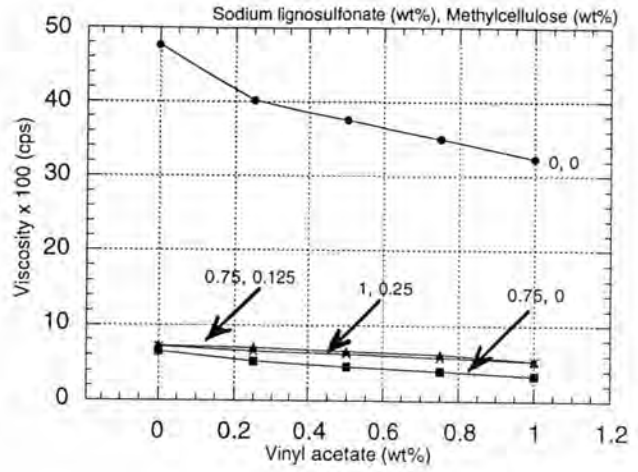

(a.)

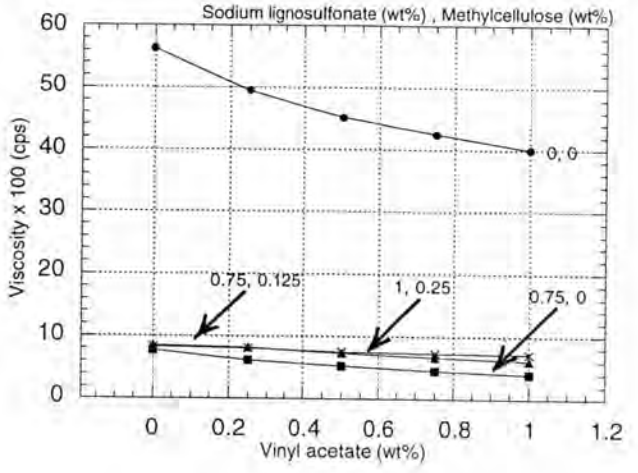

(b.)

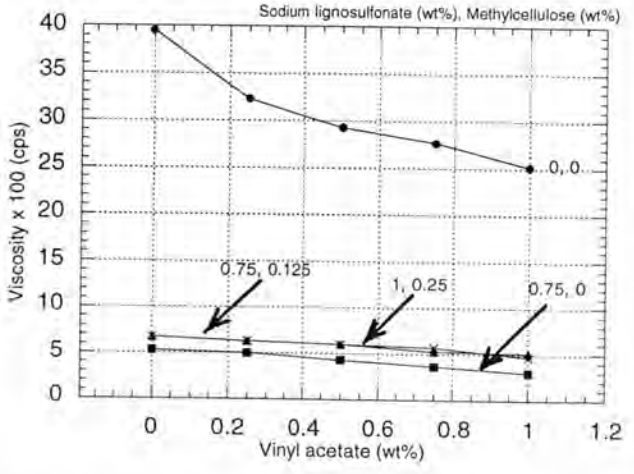

(c.)

Fig. 4.57 Relationship between the content of sodium lignosulfonate + methylcellulose + vinyl acetate and viscosity of projection plaster prepared from a.) B, b.) P and c.) NG.

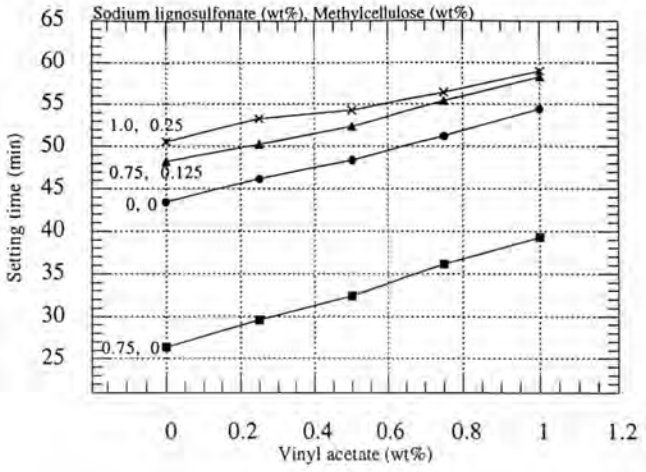

(a.)

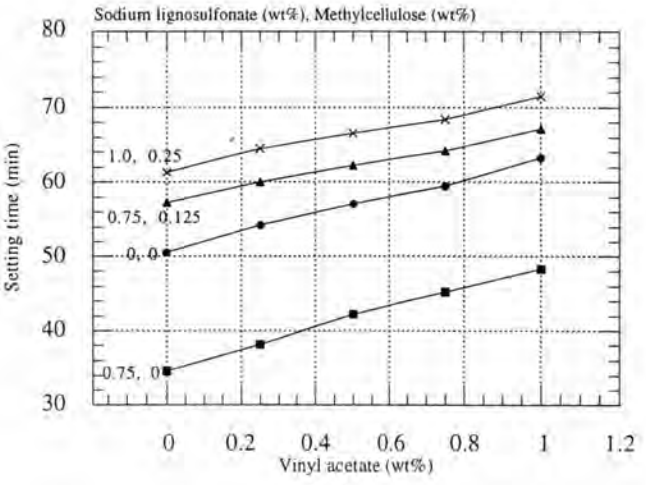

(b.)

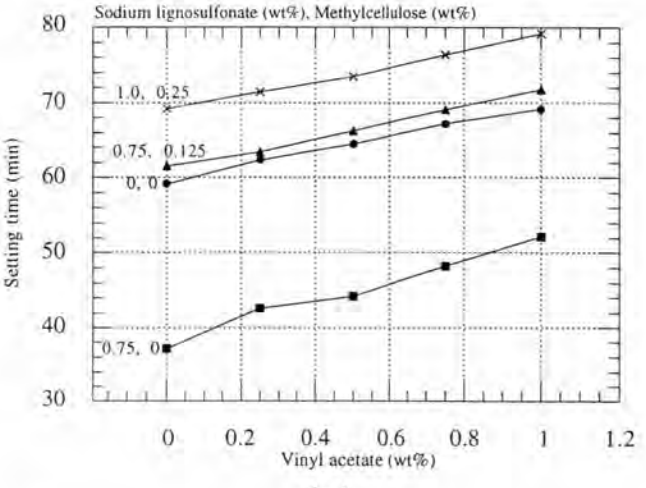

(c.)

Fig. 4.58 Relationship between the content of sodium lignosulfonate + methylcellulose + vinyl acetate and initial setting time of projection plaster prepared from a.) B, b.) P and c.) NG.

Fig. 4.57 showed that the viscosity of the projection plaster decreased with the content of vinyl acetate alone but when blended with sodium lignosulfonate and methylcellulose, the viscosity gradually decreased with the increasing in the content of vinyl acetate. This was because vinyl acetate also acted as an air-entraining material, producing a small portion of air bubbles to enhance flowability but too much of them leading to big bubbles which affected the physical properties.

Setting time of modified projection plaster was shown in Fig. 4.58. It was found that setting time increased with the content of vinyl acetate and slightly decreased when blended with sodium lignosulfonate and methylcellulose.

b.) Surface coverage and surface hardness

Effect of the content of vinyl acetate on surface coverage and surface hardness was indicated in Appendix : Table 19, page 164 and Fig. 4.59.

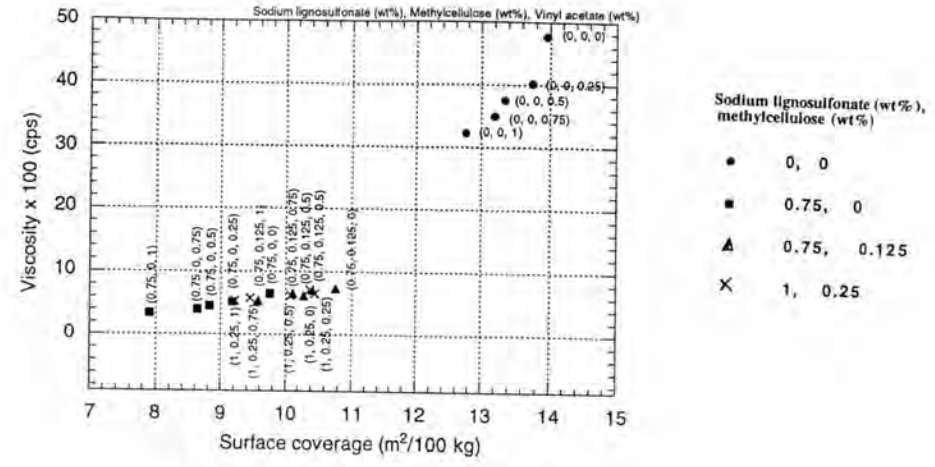

(a.)

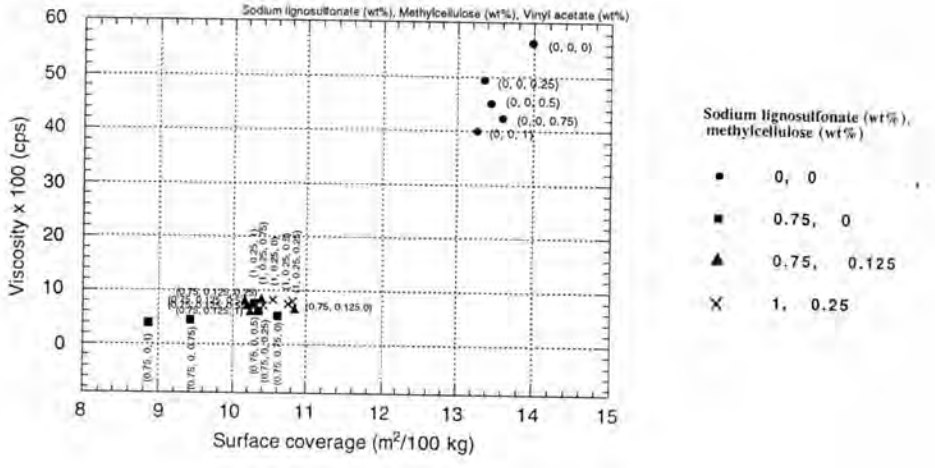

(b.)

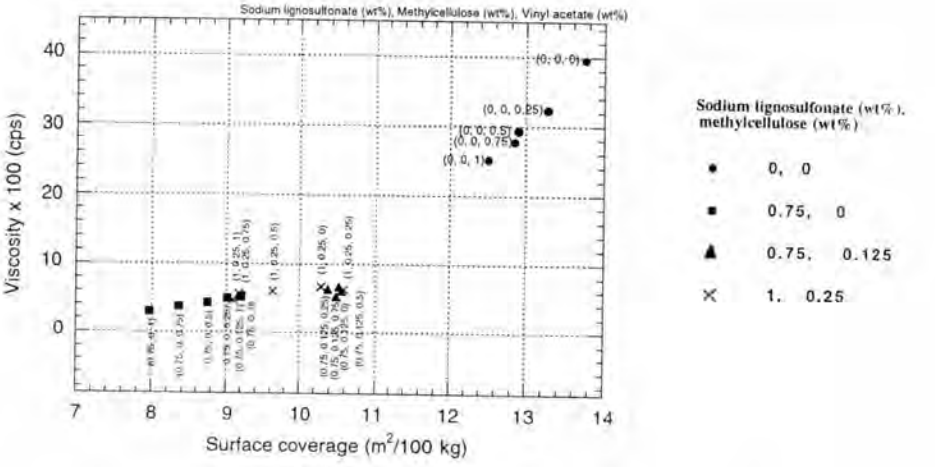

(c.)

Fig. 4.59 Relationship between viscosity and surface coverage of modified projection plaster a.) B, b.) P and c.) NG.

Fig. 4.59 showed that the results of surface coverage of projection plaster well covered the range of 9-10 m^2/100kg which conformed to DIN 1168 (Table 2.10) but some of which contained only sodium lignosulfonate and vinyl acetate was disqualified because both additives improved the flowability and gave too low viscosities, 300-500 cps. So, it was not suitable for applying as projection plaster, the suitable viscosities were 600-800 cps.

The results of surface hardness of projection plaster was tabulated in Table 4.34, it was found that surface hardness increased with the content of vinyl acetate but decreased when adding too much because it entrained big bubbles in the mixture which caused pitting on the surface of finished projection plaster.

c.) Physical properties of modified projection plaster

Effect of the content of vinyl acetate on the physical properties of projection plaster was tabulated and illustrated in Appendix : Table 20, page 165 and Fig. 4.60-4.62.

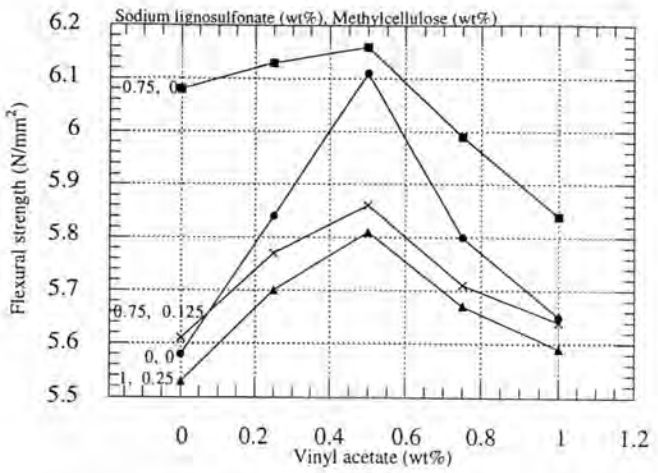

(a.)

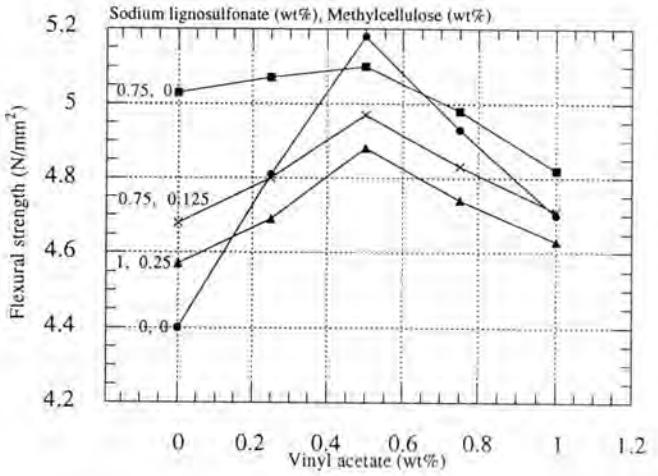

(b.)

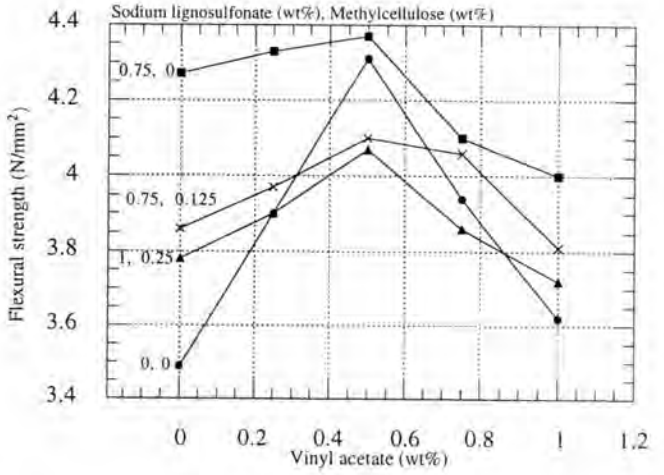

(c.)

Fig. 4.60 Relationship between the content of sodium lignosulfonate + methylcellulose + vinyl acetate and flexural strength of projection plaster prepared from a.) B, b.) P and c.) NG.

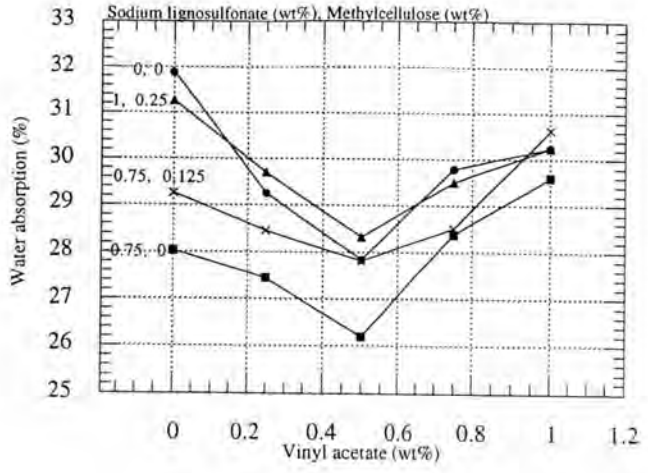

(a.)

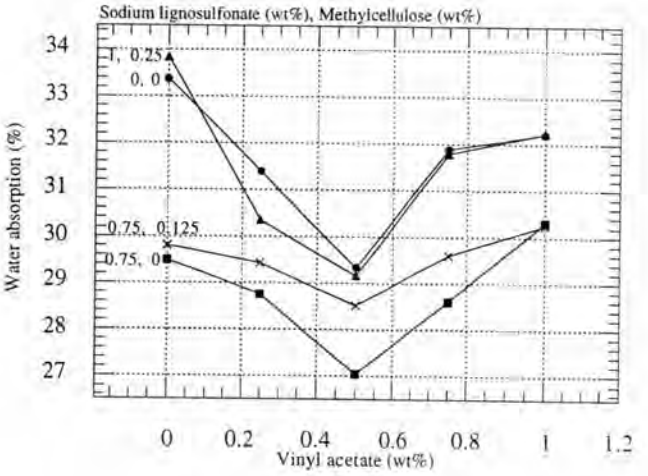

(b.)

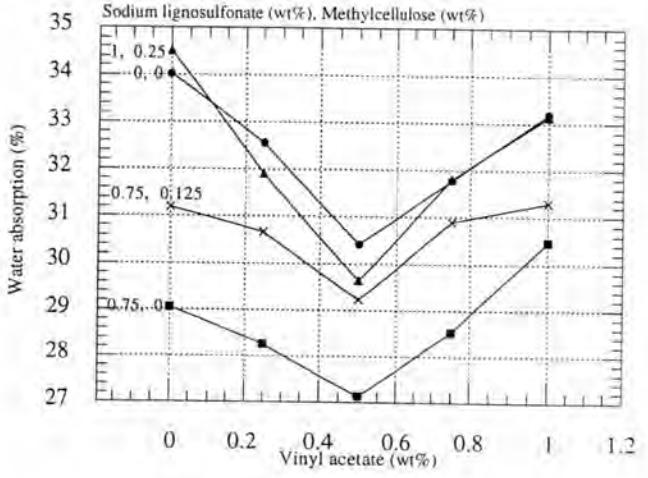

(c.)

Fig. 4.61 Relationship between the content of sodium lignosulfonate + methylcellulose + vinyl acetate and water absorption of projection plaster prepared from a.) B, b.) P and c.) NG.

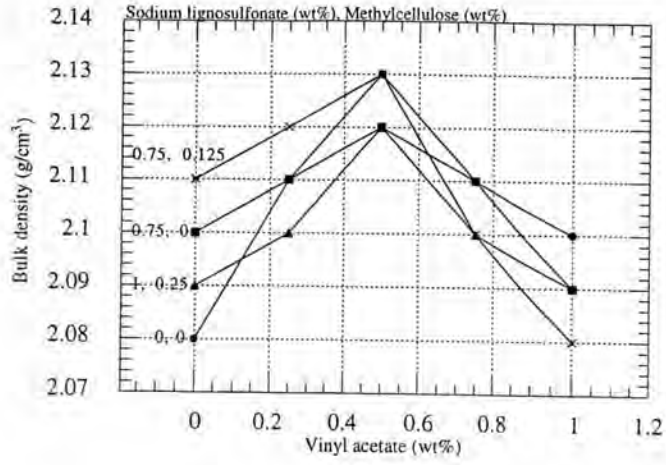

(a.)

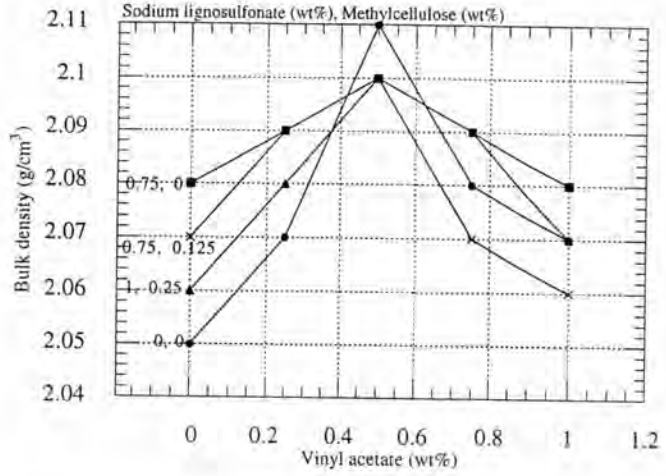

(b.)

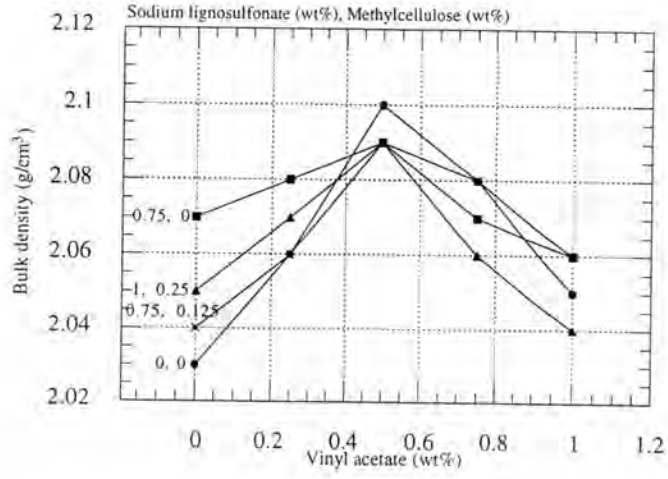

(c.)

Fig. 4.62 Relationship between the content of sodium lignosulfonate + methylcellulose + vinyl acetate and bulk density of projection plaster prepared from a.) B, b.) P and c.) NG.

Fig. 4.60 indicated that the flexural strength increased with the content of vinyl acetate and became maximum at 0.5 wt%. The drop in strength at higher contents might result from the entraining of big air bubbles in the mixture and these air bubbles made the finished specimens porous, hence lower flexural strength.

This result was also supported by the results of water absorption and bulk density (Fig. 4.61 and 4.62). It was found that the water absorption increased while the bulk density decreased when the content of vinyl acetate higher than 0.5 wt%.

In conclusion, the suitable ratio of additives chosen for the preparation of projection plaster was 0.75 wt% sodium lignosulfonate : 0.125 wt% methylcellulose : 0.50 wt% vinyl acetate, considering from its workability and typical properties. The typical properties of projection plaster with the mentioned ratio were concluded in Table 4.15.

Table 4.15 Typical properties of projection plaster with the combined additives.

Samples	ηx100 (cps.)	Surface coverage (m^2/100kg)	Setting time (min)		Flexural strength (N/mm^2)	Water absorption (%)	Bulk density (g/cm^3)	Surface hardness	
			Initial	Final				Gouge	Scratch
B	7.30±1.75	10.26±0.36	54.53±0.35	137.29±2.97	5.82±0.30	28.20±1.56	2.10±0.06	3H	HB
P	7.17±1.64	10.33±0.65	60.36±0.19	159.05±3.35	4.90±0.57	28.57±1.75	2.10±0.05	2H	HB
NG	6.70±1.76	10.45±0.51	61.25±0.32	140.11±3.45	4.05±0.42	30.38±1.84	2.07±0.04	2H	B

* the number of each test was 5.